Science Arts & Métiers (SAM)

To cite this version :

Claude FENDZI, Nazih MECHBAL, Mikhail GUSKOV, Marc RÉBILLAT - A General Bayesian Framework for Ellipse-based and Hyperbola-based Damage Localisation in Anisotropic Composite Plates - Journal of Intelligent Material Systems and Structures - Vol. 27, n°3, p.350-374 - 2016

A General Bayesian Framework for Ellipse-based and Hyperbola-based Damage Localisation in Anisotropic Composite Plates

C. Fendzi[1], **N. Mechbal**[1], **M. Rébillat**[1], **M. Guskov**[1], and **G. Coffignal**[1]

[1] PIMM Laboratory, UMR CNRS 8006 Arts et Métiers ParisTech,
151 Boulevard de l'Hôpital 75013, Paris, France

claude-marcellin.fendzi-tefoit@ensam.eu

Abstract

This paper focuses on Bayesian Lamb wave-based damage localization in structural health monitoring of anisotropic composite materials. A Bayesian framework is applied to take account for uncertainties from experimental time-of-flight measurements and angular dependent group velocity within the composite material. An original parametric analytical expression of the direction dependence of group velocity is proposed and validated numerically and experimentally for anisotropic composite and sandwich plates. This expression is incorporated into time-of-arrival (ToA: ellipse-based) and time-difference-of-arrival (TDoA: hyperbola-based) Bayesian damage localization algorithms. This way, the damage location as well as the group velocity profile are estimated jointly and a priori information taken into consideration. The proposed algorithm is general as it allows to take into account for uncertainties within a Bayesian framework, and to model effects of anisotropy on group velocity. Numerical and experimental results obtained with different damage sizes or locations and for different degrees of anisotropy validate the ability of the proposed algorithm to estimate both the damage location and the group velocity profile as well as the associated confidence intervals. Results highlight the need to consider for anisotropy in order to increase localization accuracy, and to use Bayesian analysis to quantify uncertainties in damage localization.

Keywords: Structural health monitoring, damage localization, Lamb waves, anisotropic composite materials, Bayesian framework, Markov Chain Monte Carlo method.

1   Introduction

Structural Health Monitoring (SHM) is an emerging technology that aims at designing systems able to continuously monitor structures (Sohn et al., 2003). One commonly used SHM technique is that of "active sensing" whereby permanently attached actuators launch Lamb waves in the structure under inspection and a set of sensors records the structural responses in order to extract some damage related information (Farrar et al., 1999; Giurgiutiu, 2005; Lin and Yuan, 2001). One of the

1

outstanding advantage of using Lamb waves for SHM is that such waves can travel over relatively long distance and can be used to monitor various types of damage (delaminations, disbonds, fiber breaking, impact, holes, etc...). However, phenomena like dispersion and anisotropy (dependence of the wave velocity with respect to frequency and propagation direction), mode conversion (change in wave velocity when wave interacts with structural discontinuities or boundaries) as well as changing environment and operational conditions make reliable damage localization a challenging task.

For damage localization, each piezoelectric element attached to the structure acts as an actuator while the others are used as sensors. Performing the difference between signals recorded on healthy and damaged states, a scattered signal containing information related to the damage (location, size, orientation, type) is obtained (Yu et al., 2012). Time-of-flight (ToF), which corresponds to the time taken by the wave packet to travel from an actuator to a sensor through a given path, is a feature extracted from the scattered signal that is widely used for damage localization (Flynn et al., 2011; Ihn and Chang, 2008; Lu et al., 2006; Michaels, 2008; Moll et al., 2010; Su and Ye, 2009). Knowing the ToF values and the wave velocity, the damage localization problem becomes straightforward: solve a set of deterministic nonlinear equations that describe the relationship between the coordinates of the damage, the ToF, and the wave velocity. Two kind of equations can be used to do so: those relying on time-of-arrival (ToA) and provide damage location as the intersection of several ellipses and other based on time-difference-of-arrival (TDoA) and provide damage location as the intersection of hyperbolas. Many authors have successfully used these strategies for damage localization (Coverley and Staszewski, 2003; Flynn et al., 2011; Michaels, 2008; Su and Ye, 2009). However, to the knowledge of the authors, the influence of the use of ToA of DToA on localization accuracy has yet not been addressed and thus constitutes the first issue discussed in this paper.

As stated above, a model involving the waves group velocity linking the damage position and the ToFs is necessary to achieve accurate localization. Modelling Lamb wave propagation in isotropic composite plates at a given frequency is relatively simple as only a direction independent group velocity is involved. However, for composite anisotropic plate-like structures, such a model is much more complicated to establish. Indeed, in case of anisotropic plates the wave velocity is now a function of the propagation angle and not a single value (Li et al., 2013). Several techniques have been proposed to overcome this difficulty. In general, these techniques fall in two groups. The first group deals with strategies in which the group velocity profile (Coverley and Staszewski, 2003; Hajzargerbashi et al., 2011; Kundu et al., 2007) is assumed to be known. The second group includes strategies based on clusters of sensors (sensors are regrouped by zone) in which the knowledge of the group velocity profile is not required (Ciampa and Meo, 2010; Kundu et al., 2012). The assumption behind those strategies is that sensors located in the same cluster have the same group velocity. Following the methods of the first group, the second point addressed in this paper is to propose and validate an efficient and simple parametric modeling of the group velocity profile in order to deal easily with anisotropy.

Finally, ToF measurements error may arise due to experimental noise, and may corrupt the damage localization results (Niri et al., 2013; Niri and Salamone, 2012). Strategies are thus also needed to take into account for these uncertainties. To face parts of this problem, some Bayesian approaches have already been developed. The advantage of the Bayesian methodology, is that expert judgments or knowledge can be incorporated into the Bayesian model as prior information to reduce the variance error. Many authors have previously used Bayesian estimation to update the belief in the parameter estimation results in various field of engineering (Beck and Au, 2002; Beck and Katafygiotis, 1998; Vanik et al., 2000). For some years now, Bayesian approaches play

a key role in SHM. They have been applied for damage assessment (Jiang and Mahadevan, 2008), damage prediction (Karandikar et al., 2012), sensor placement optimization (Flynn and Todd, 2010), etc. Regarding damage localization, Zhao et al. (2007) combined a probabilistic approach with a tomography-based damage imaging method to improve damage localization accuracy. Flynn et al. (2011) proposed a maximum likelihood estimation (MLE) of damage location in an aluminium plate. Yu and Su (2012) proposed an application of kernel density estimation in order to account for the uncertainties in ToF measurements in an aluminium plate. A non-parametric estimation is performed to draw a probabilistic distribution of the ToF data in order to improve the damage localization. Recently, Niri and Salamone (2012) proposed a probabilistic approach based on an extended Kalman filter approach (EKF) for acoustic source localization in composite anisotropic panels. They take into account uncertainties in both ToF measurements and group velocity. Yan (2013) proposed a Bayesian system identification for damage localization in plate-like structure using Lamb waves. This approach also takes into account uncertainties in ToF measurement and group velocity. All these studies are however limited to the particular isotropic case where the group velocity is not a function of the angle of propagation, which is not the case for anisotropic materials, as stated above. The third point addressed by this paper is the use of a probabilistic framework in order to take into account for both measurement and material uncertainties in an anisotropic context.

On the basis of the framework developed by Yan (2013), we propose a general localization algorithm that allows (i) to take into account for for both measurement and material uncertainties within a Bayesian framework, (ii) to model easily the effects of anisotropy on group velocity and, (iii) to rely on ToA or TDoA informations. The original feature of this approach is that it incorporates anisotropic wave propagation via a parametrized analytic expression of the angle dependence of the wave velocity profile in the Bayesian localization model and allows to use both ToA and TDoA informations. Using this algorithm we highlight the need to take into account for anisotropy in order to achieve accurate damage localization and compare the efficiency of the use of ToA and DToA information for damage localization.

The paper is organized as follows: Section 2 introduces the background of damage localization in anisotropic plates. The parametric expression of the group velocity profile proposed here is detailed in Section 3 and validated in Section 4. In Section 5, the Bayesian framework and the Markov Chain Monte Carlo (MCMC) method used to solve it are presented. Numerical and experimental results are presented in Section 6 for an anisotropic composite plate before drawing a conclusion in Section 7.

2 Lamb waves-based damage localization in composite plates

Lamb waves-based damage localization in structures is based on the fundamental idea that a traveling wave in a damaged plate will be scattered by the damage (Su and Ye, 2009). Performing the difference between signals recorded on healthy and damaged states, a scattered signal containing information related to the damage (location, size, orientation, type) is obtained. Time-of-flight (ToF), which corresponds to the time taken by the wave packet to travel from an actuator to a sensor through a given path, is a feature extracted from the scattered signal that is widely used for damage localization (Flynn et al., 2011; Ihn and Chang, 2008; Lu et al., 2006; Michaels, 2008; Moll et al., 2010; Su and Ye, 2009) as detailed in Section 2.1. ToF algorithms usually fall within two groups: the ToA-based algorithm (ellipse method, see Section 2.2) and the TDoA-based algorithm (hyperbola method, see Section 2.3) (Flynn et al., 2011; Moll et al., 2010) that are brielfy presented in the following.

2.1 Time-of-Flight (ToF) estimation

ToF estimation is an important issue in Lamb wave-based damage localization, since uncertainties in measurements can affect localization accuracy (Niri et al., 2013; Niri and Salamone, 2012; Yan, 2013). To tackle this problem, a variety of methods have been developed. Commonly used methods include short-time Fourier transform (STFT), Hilbert-Huang transform (HHT), matching pursuit decomposition (MPD), Wigner-Ville distribution (WVD), cross-correlation method (CCM), Hilbert transform (HT), and continuous wavelet transform (CWT) (Jeong and Jang, 2000; Niethammer et al., 2001; Raghavan and Cesnik, 2007; Tua et al., 2004; Xu et al., 2009). In this study, CWT was used to perform time-frequency decomposition of the scattered signal in order to extract the component of the signal corresponding to the frequency of interest. CWT is a band-pass filtering procedure in which the signal is convolved with the wavelet centered on the driving frequency. Thereafter, HT was used to estimate ToF by extracting the time of the first maximum of the envelope of the signal component at the frequency of interest.

2.2 Time of arrival (ToA): ellipse method

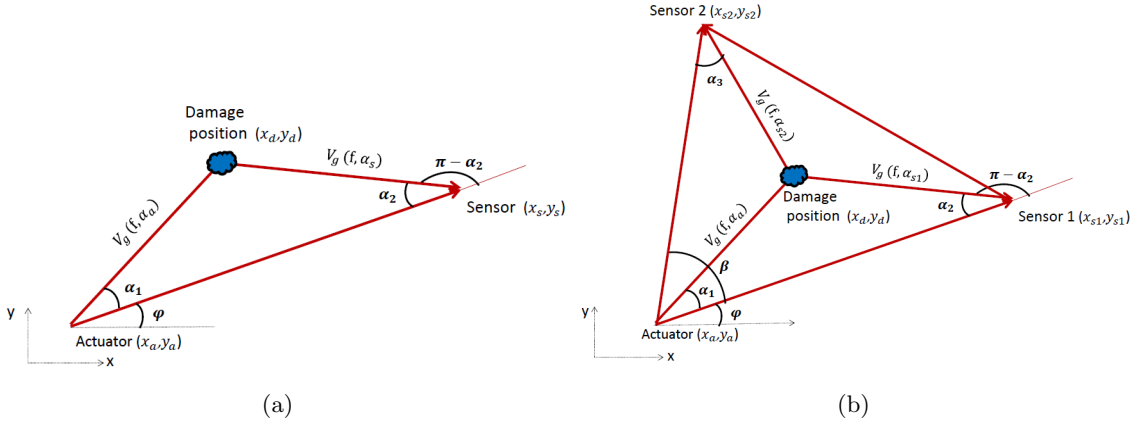(a)   (b)

Figure 1: Damage localization in anisotropic plate-like structures: (a) Ellipse method, (b) Hyperbola method.

Consider a transducers network with N piezoelectric elements bonded on the plate. Each transducer can act as both actuator and sensor. The geometric relationship for damage localization in plate-like structures using ToA model is schematically shown in Figure 1(a) for a single piezoelectric actuator-sensor pair. The coordinates of the actuator are (x_a, y_a), and (x_s, y_s) for the sensor. When a wave travels from the actuator across a point-like damage to the sensor, the ToA of the scattered signal corresponds to the wave travel time of the actuator-damage-sensor path and can be expressed as (Ihn and Chang, 2008; Michaels, 2008) :

$$\text{ToA}^{a-s} = \frac{\sqrt{(x_d - x_a)^2 + (y_d - y_a)^2}}{V_g(f, \alpha_a)} + \frac{\sqrt{(x_d - x_s)^2 + (y_d - y_s)^2}}{V_g(f, \alpha_s)} \tag{1}$$

where (x_d, y_d) is the damage coordinate, $V_g(f, \alpha)$ is the group velocity of the Lamb wave, which depends on the frequency f, and the propagation direction in composite material α. $V_g(f, \alpha_a)$ and $V_g(f, \alpha_s)$ represent the group velocity in the actuator-damage path and damage-sensor path

respectively. In the model given by Equation (1), the sizes of the actuator, sensor, and damage area are not taken into account. For isotropic material, group velocity is angular independent and the solution of Equation (1) is an ellipse for each actuator-sensor pair, and the damage location corresponds to the intersection point of all ellipses for all actuators sensors paths (Yan, 2013). The problem is more complicated for anisotropic materials since the group velocity of the interrogating waves depends on the propagation direction (Ciampa and Meo, 2010).

2.3 Time difference of arrival: hyperbola method

The time difference of arrival (TDoA) method considers piezoelectric elements in groups of three with one acting as an actuator (noted a) and the others two as sensors (noted s_1 and s_2). If there is a damage at the point (x_d, y_d), the difference in the times of arrival of the scattered signals at the two sensors is (Michaels, 2008; Moll et al., 2010):

$$\Delta\text{ToA}^{s_1-s_2} = \text{ToA}^{a-s_1} - \text{ToA}^{a-s_2} \tag{2}$$

Since the distance from the actuator to the damage is the same for both receivers (Figure 1(b)), it does not affect the difference in arrival time. Equation (2) can then be simplified as:

$$\Delta\text{ToA}^{s_1-s_2} = \frac{\sqrt{(x_d - x_{s_1})^2 + (y_d - y_{s_1})^2}}{V_g(f, \alpha_{s_1})} - \frac{\sqrt{(x_d - x_{s_2})^2 + (y_d - y_{s_2})^2}}{V_g(f, \alpha_{s_2})} \tag{3}$$

where (x_{s_i}, y_{s_i}) is the coordinate of the sensor i, $V_g(f, \alpha_{s_i})$ is the group velocity and α_{s_i} is the angle of propagation in the direction damage-sensor i ($i = 1, 2$). Solution of Equation (3) is a hyperbola, and the damage location is obtained as the point of intersection of all the hyperbolas obtained for all the possible triplets (a, s_i, s_j) in the transducers network, with $i \neq j$. As in the ellipse method, the angular dependence group velocity complicates the resolution of this equation.

3 Modeling the group velocity profile in an anisotropic composite plate

As aforementioned, the damage location is obtained by solving the set of nonlinear equations given by Equations (1) or (3). For anisotropic structures equipped with N piezo-electric elements, a unique solution for this set of nonlinear equations cannot be found because the number of equations ($N - 1$) is lower than the number of unknowns ($N + 2$) that are: the damage location coordinates (x_d, y_d) and N angular dependent group velocities $V_g(\alpha_i)$. Several techniques that falls in two groups have been proposed to overcome this difficulty. The first group deals with strategies in which the group velocity profile (Coverley and Staszewski, 2003; Hajzargerbashi et al., 2011; Kundu et al., 2007) is assumed to be known. The second group includes strategies based on clusters of sensors (sensors are regrouped by zone) in which the knowledge of the group velocity profile is not required (Ciampa and Meo, 2010; Kundu et al., 2012). The assumption behind those strategies is that sensors located in the same cluster have the same group velocity. Here, we propose to follow the first group of methods and to use a model of the group velocity profile in order to decrease the number of unknown coefficients in the localization equations given by Equations (1) and (3).

3.1 Typical group velocity profile in anisotropic composite plates

Before modeling the group velocity profile for an anisotropic composite plate, an example of such a profile is shown. The chosen anisotropic composite is a 4 plies composite lamina with plies orientation $[0°/-45°/45°/0°]$ and a 0.28 mm thickness typically used in aeronautic applications. Mechanical properties of one ply of the composite material are listed in Table 1.

Table 1: Mechanical properties of one ply of the chosen composite material

Density (g/m^3)	thickness (mm)	E_{11} (GPa)	E_{22} (GPa)	E_{33} (GPa)	$G_{12} = G_{13} = G_{23}$ (GPa)	ν_{12}
1554	0.28	60	40	8.1	4.8	0.03

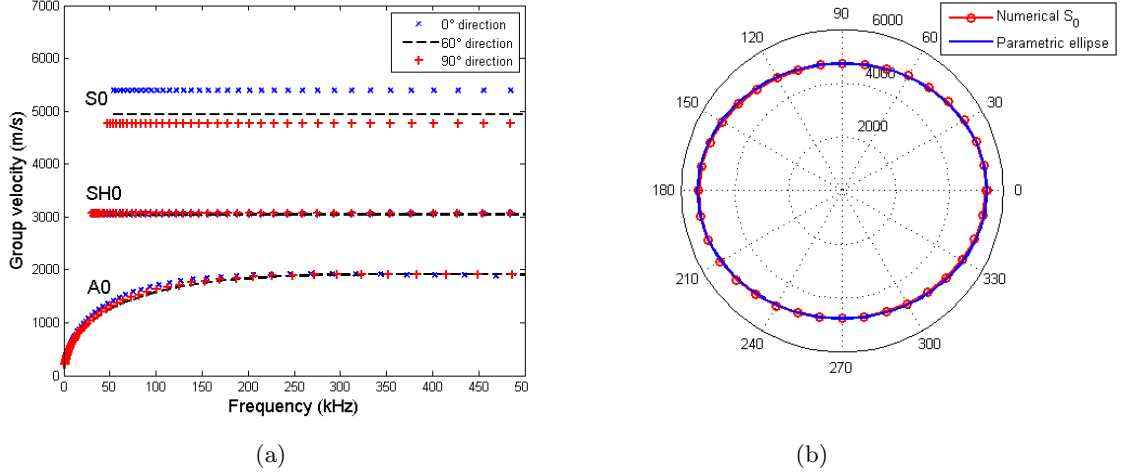
(a)   (b)

Figure 2: (a) Dispersion curves for different directions. (b) Numerical and approximated velocity profile for the S0 Mode at 150 kHz.

Numerical studies have been conducted on the selected composite using SDTools (Balmes, 2014), a finite element toolbox developed in MATLAB environment. The objective was to compute Lamb wave dispersion curves for the composite plate (Table 1). Thereby, the dispersion curves were computed using periodic computations (Macea et al., 2005; Sorohan et al., 2011). The dispersion curves are computed only in the low frequency domain, where exist the fundamental antisymmetric Lamb wave mode, A_0, symmetric Lamb wave mode, S_0, and the lowest order shear horizontal SH_0 wave mode. Figure 2(a) shows the dispersion curves along different directions of propagation ($0°$, $60°$ and $90°$) with respect to the fiber direction. It can be observed that, the wave mode S_0 exhibits reasonably non-dispersive behavior with a nearly constant group velocity and that this mode is the faster one. Furthermore, this wave mode has been recognized to be more sensitive to through-thickness defect (Su and Ye, 2009), which is the type of defect considered in this study. As a result, the wave mode S_0 at 150 kHz is chosen for damage localization. From the dispersion curves, the velocity profile of the S_0 mode can be determined at 150 kHz and plotted in a polar coordinate system as shown in Figure 2(b). The polar axis represents the propagation angle with respect to the principal material axis. As it can be seen from this figure, there is indeed variation of the group velocity with the propagation angle within this material. Furthermore, since the group velocity profile has an identifiable geometrical shape, a parametric curve can be derived to approximate this velocity profile.

3.2 Proposed parametric ellipse model of the group velocity profile

In order to approximate the angle dependence group velocity profile for the S_0 mode shown in Figure 2(b), we proposed the following parametric ellipse expression:

$$V_g(\gamma) = \sqrt{V_{g_x}^2 + V_{g_y}^2} = \sqrt{[a\cos(\gamma)]^2 + [b\sin(\gamma)]^2} \tag{4}$$

where the physical angle α (for each actuator-sensor path, see Figure 1) is related to the parameter angle γ by the expression:

$$\alpha = \arctan\left(\frac{V_{g_y}}{V_{g_x}}\right) = \arctan\left(\frac{b}{a}\tan(\gamma)\right) \tag{5}$$

hence,

$$\gamma = \arctan\left(\frac{a}{b}\tan(\alpha)\right) \tag{6}$$

where γ varies from 0 to 360°. In the above expression the two parameters a and b can be estimated using the minimum and maximum values of the group velocity data. The values for parameters **a** and **b** are **5395.5 m/s** and **4761.3 m/s** respectively. The approximated velocity profile based on the parametric ellipse is shown in Figure 2(b). One can observe an excellent match between numerical group velocity data and the proposed parametric ellipse form. This agreement shows the validity of the proposed parametric function for velocity profile approximation for this material at 150 kHz. The advantage of using this model is to reduce the number of parameters involved in the group velocity profile to only two, whatever the number of sensors that are considered.

Including this model within the ToA and DToA methods presented in Sections. 2.2 and 2.3, and according to the chosen geometry, we then obtain:

- ToA (ellipse method), see Figure 1(a):

$$\alpha_a = \varphi + \alpha_1 \quad \text{and} \quad V_g(f, \alpha_a) = V_g(\gamma_a) \quad \text{with} \quad \gamma_a = \arctan\left(\frac{a}{b}\tan(\alpha_a)\right)$$

$$\alpha_s = \varphi + \pi - \alpha_2 \quad \text{and} \quad V_g(f, \alpha_s) = V_g(\gamma_s) \quad \text{with} \quad \gamma_s = \arctan\left(\frac{a}{b}\tan(\alpha_s)\right) \tag{7}$$

- TDoA (hyperbola method), see Figure 1(b):

$$\alpha_{s_1} = \varphi + \pi - \alpha_2 \quad \text{and} \quad V_g(f, \alpha_{s_1}) = V_g(\gamma_{s_1}) \quad \text{with} \quad \gamma_{s_1} = \arctan\left(\frac{a}{b}\tan(\alpha_{s_1})\right)$$

$$\alpha_{s_2} = \varphi + \beta + \alpha_3 \quad \text{and} \quad V_g(f, \alpha_{s_2}) = V_g(\gamma_{s_2}) \quad \text{with} \quad \gamma_{s_2} = \arctan\left(\frac{a}{b}\tan(\alpha_{s_2})\right) \tag{8}$$

4 Validation of the proposed parametric expression of the group velocity profile for damage localization in a deterministic framework

As stated above, a model involving the wave group velocity that links the damage position and the ToFs is necessary to achieve accurate localization. An efficient and simple parametric modeling of the group velocity profile able to deal easily with anisotropy has been presented in the previous section. This section will now highlight in a deterministic framework the need to take into account for anisotropy in order to increase localization accuracy and thus the benefits associated with this simple model.

4.1 Finite element model

The same $[0°/45°/-45°/0°]$ composite laminate described previously is used here. A set of $N = 5$ piezoelectric (PZT) elements (Noliac NCE51) from NOLIAC Inc., each with a diameter of 20 mm and thickness of 0.1 mm are surface-mounted on the composite plate. Each piezoelectric element can act both as actuator and sensor. An illustration of the plate and sensor placement is shown in Figure 3. The coordinates of the piezoelectric elements and of the damage are listed in Table 2.

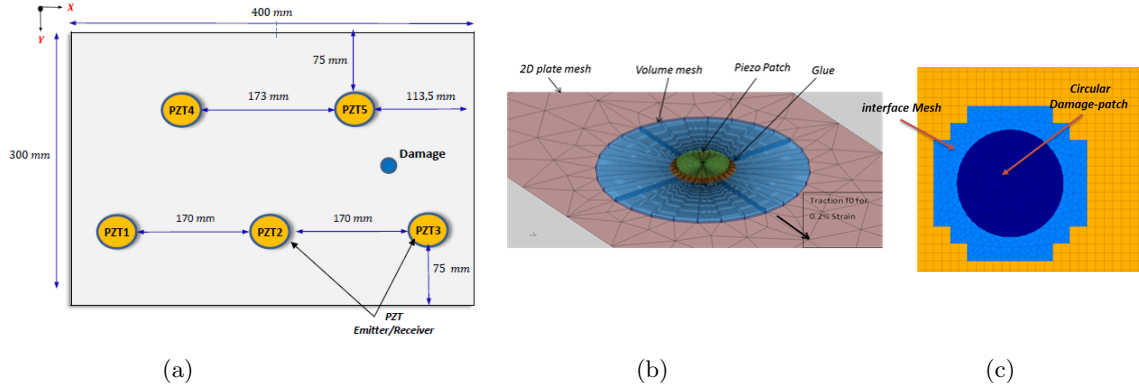(a)   (b)   (c)

Figure 3: (a) Schematic view of the composite plate with a damage. (b) Meshing of the PZT. (c) Meshing of the Damage

Table 2: Coordinates of the piezoelectric elements

	PZT_1	PZT_2	PZT_3	PZT_4	PZT_5	Damage
x (mm)	30	200	370	113.5	286.5	300
y (mm)	75	75	75	225	225	160

To perform damage localization, numerical simulations are conducted using SDTools. Squared elements with dimension 2 mm $\times$ 2 mm were used for the meshing. This mesh size is compatible with the propagating wavelength of the S_0 mode which value is 8 mm at 150 kHz. The excitation signal is chosen as a 5 cycles sinusoidal tone burst at a central frequency of $f_0 = 150$ kHz, which is modulated by a Hanning window. The time step for the transient simulation is 0.3 μs chosen as sampling period whose sampling frequency is 3.33 MHz. The damage has a circular shape with 20 mm of diameter. The damage is represented by a reduction of material properties (a reduction of rigidity of 90%) in a chosen area as shown in Figure 3(c). To introduce it, an automatic approach has been developed where a damage-patch is generated with a specific mesh. The dimension and the material properties of this damage-patch can be changed and adjusted. The introduction of this patch before changing its properties does not alter the modal properties of the structure in the frequency range of interest. Moreover, nodes inside this damage-patch could be removed to create crack or hole damages. The center location of the damage is (300,160) mm. Details of the FEM model with the meshing of the PZT and the damage are shown in Figures 3(b)(c). It is worth mention that this FEM model was validated through experiments conducted on the same specimens (Balmes et al., 2014).

8

4.2 Signal processing and ToF extraction

The signal scattered from damage is extracted by performing the difference of signals between the healthy and damaged plate for each PZT. In order to extract ToF information from the scattered signal, a CWT Gabor wavelet is chosen for the data processing (see Section 2.1). Thereafter a Hilbert transform is applied to the processed signal in order to extract its envelope and thus, the ToF information. The processed scattered signal and its Hilbert transform are shown in Figure4.
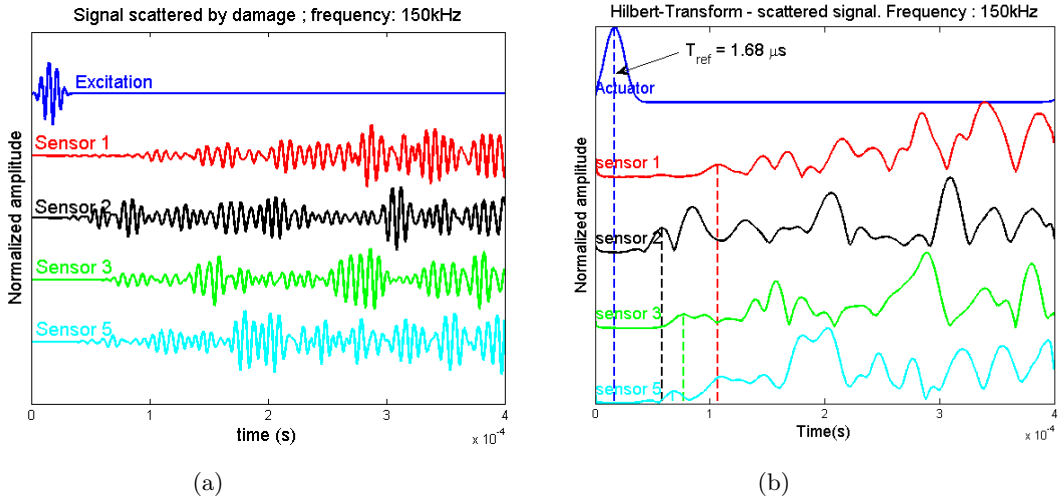

(a) (b)

Figure 4: Signals scattered by damage -numerical study- (a) and the Hilbert transform (b) at central frequency of 150 kHz when PZT 4 acts as actuator. The ToF from actuator to the sensors is represented by vertical dashed lines. The starting time for the ToF calculation is labeled as T_{ref}.

4.3 Damage localization results

Assuming each node in the composite plate as a possible damage location, theoretical ToA or DToA can be computed at each node (x, y) knowing the group velocity by means of Equations (1) or (3). This procedure is repeated for each node and each actuator sensor path, and a damage index $P(x, y)$ at any node (x, y) is obtained by comparing the theoretical ToA or DToA $t_i^{\mathrm{TH}}(x, y)$ to the data extracted from scattered signal t_i^{XP} as follows:

$$P(x, y) = \sum_{i=1}^{N_p} \exp\left[-\frac{|t_i^{\mathrm{TH}}(x, y) - t_i^{\mathrm{XP}}|}{\tau_0}\right] \tag{9}$$

where N_p is the total number of actuator sensor pathes and τ_0 is a decay factor playing the role of a decay rate of an exponential windowed function applied to reduce secondary reflections of the scattered signal; its value is fixed at 5 μs in this study. The estimated damage location is then chosen as the point having the maximum value of $P(x, y)$. In order to highlight the need to account for anisotropy, localization is performed using both the approximate proposed velocity profile and an isotropic model that assumes that velocities along different directions are the same and equal to the average velocity across all angles.

Figure 5 shows the localization result for both ellipse and hyperbola methods and when taking account for anisotropy or not. Black circle represents actual damage position and white circle

9

represent the estimated damage location. Localization results for both methods and with and without anisotropy are listed in Table 3. From Figure 5 and Table 3, it can be seen that both methods provide accurate localization results and that the ellipse-based method appears to be slightly more accurate for this example. We can notice that taking account for anisotropy allows to greatly increase the localization accuracy and to reduce localization ambiguities.
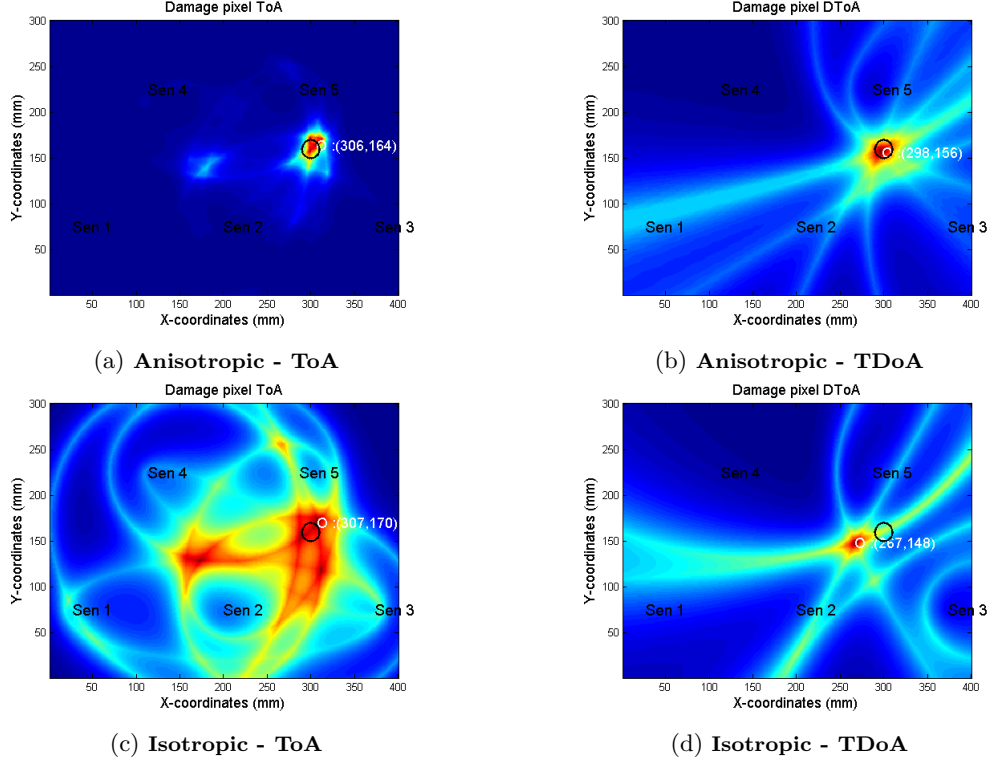

(a) **Anisotropic - ToA**

(b) **Anisotropic - TDoA**

(c) **Isotropic - ToA**

(d) **Isotropic - TDoA**

Figure 5: Damage localization results - numerical study - : (a) ellipse method using the proposed parametrized group velocity profile,(b) hyperbola method using the proposed parametrized group velocity profile, (c) ellipse method using an isotropic velocity profile, and (d) hyperbola method using an isotropic velocity profile.

5 Bayesian approach for damage localization

We then consider the use of a probabilistic framework in order to take into account for both measurement and material uncertainties which have been ignored in the anisotropic context developed in the previous section. Rather than a single damage location, the Bayesian approach will provide a probability density function of the unknown parameters (that includes damage location), with a mean and a confidence interval (Yan, 2013; Yu and Su, 2012). In the present damage localization problem, the parameter vector is in general $\boldsymbol{\theta} = [x_d, y_d, V_g(f, \alpha_a), V_g(f, \alpha_s)]$ for each actuator-damage-sensor path. Considering the parametric elliptical form for the group velocity profile described in section 3.2 this parameter vector can be simplified as $\boldsymbol{\theta} = [x_d, y_d, a, b]$.

Table 3: Estimated location and errors for the damage position $(300, 160)$ in mm

	Anisotropic model				Isotropic model			
	ToA method		TDoA method		ToA method		TDoA method	
Coordinates	x_d	y_d	x_d	y_d	x_d	y_d	x_d	y_d
Estimation (mm)	299	159	295	159	272	165	279	149
Error (mm)	1	1	5	1	28	-5	21	11

5.1 Probabilistic description of ToF

In this part we introduce the probabilistic model describing the ToF data and the associated measurement uncertainties for both ToA-based and TDoA-based algorithm.

5.1.1 Ellipse method

Let's assume that the measurements uncertainties are described by ϵ_1, a zero-mean Gaussian random variable with variance $\sigma_{\epsilon_1}^2$. The probabilistic description of the measured ToA for the ith actuator-sensor path $\text{ToA}_m^{a-s_i}$ can be expressed as:

$$\text{ToA}_m^{a-s_i} = \text{ToA}_c^{a-s_i}(\boldsymbol{\theta}) + \epsilon_1 \tag{10}$$

where $\text{ToA}_c^{a-s_i}(\boldsymbol{\theta})$ is the calculated ToA in the ith actuator-sensor path using Equation (1), with parameter vector $\boldsymbol{\theta}$. We then obtain :

$$\epsilon_1 \sim \mathcal{N}(0, \sigma_{\epsilon_1}^2) = \frac{1}{\sigma_{\epsilon_1}\sqrt{2\pi}} \exp\left(\frac{(\text{ToA}_m^{a-s_i} - \text{ToA}_c^{a-s_i}(\boldsymbol{\theta}))^2}{2\sigma_{\epsilon_1}^2}\right)$$

The likelihood function $p_1(\boldsymbol{D}|\boldsymbol{\theta}, \sigma_{\epsilon_1}^2)$ is a probabilistic statement about the distribution of the measured ToA data $\boldsymbol{D} = [\text{ToA}_m^{a-s_1}, ..., \text{ToA}_m^{a-s_{N_p}}]$, given the predicted ToA values provided by Equation (1) and parameter vector $\boldsymbol{\theta}$. N_p is the total number of actuator-sensor paths in the transducers network. Assuming conditional independence of the time-of-flight measurements for each actuator-sensor path given the damage location, the fused likelihood function can be expressed as the product of the individual likelihoods associated with each ToA:

$$p_1(\boldsymbol{D}|\boldsymbol{\theta}, \sigma_{\epsilon_1}^2) = \prod_{i=1}^{N_p} \frac{1}{\sigma_{\epsilon_1}\sqrt{2\pi}} \exp\left(\frac{(\text{ToA}_m^{a-s_i} - \text{ToA}_c^{a-s_i}(\boldsymbol{\theta}))^2}{2\sigma_{\epsilon_1}^2}\right) = \frac{1}{(2\pi\sigma_{\epsilon_1}^2)^{N_p/2}} \exp\left(-\frac{Q_1(\boldsymbol{D}, \boldsymbol{\theta})}{2\sigma_{\epsilon_1}^2}\right)$$

where

$$Q_1(\boldsymbol{D}, \boldsymbol{\theta}) = \sum_{i=1}^{N_p}(\text{ToA}_m^{a-s_i} - \text{ToA}_c^{a-s_i}(\boldsymbol{\theta}))^2$$

5.1.2 Hyperbola method

As aforementioned, hyperbola methods uses a set of 3 piezoelectric elements, one acting as actuator and the two others as sensors. The probabilistic description of the measured TDoA between sensors i, j $(i \neq j)$ can again be expressed as:

$$\text{TDoA}_m^{s_i-s_j} = \text{TDoA}_c^{s_i-s_j}(\boldsymbol{\theta}) + \epsilon_2 \tag{11}$$

where $\text{TDoA}_c^{s_i-s_j}(\boldsymbol{\theta})$ is the calculated TDoA for sensors pair i, j using Equation (3), with parameter vector $\boldsymbol{\theta}$. Note that in parameter vector $\boldsymbol{\theta}$, the group velocity correspond to the propagation angle between actuator-sensor i and actuator-sensor j paths respectively. Assuming ϵ_2 be a zero-mean Gaussian random variable with variance $\sigma_{\epsilon_2}^2$ and following the same approach as in the case of ellipse method, with conditional independence of the time-of-flight measurements, the fused likelihood function can be written as :

$$p_2(\boldsymbol{D}|\boldsymbol{\theta}, \sigma_{\epsilon_2}^2) = \frac{1}{(2\pi\sigma_{\epsilon_2}^2)^{N_t/2}} \exp\left(-\frac{Q_2(\boldsymbol{D}, \boldsymbol{\theta})}{2\sigma_{\epsilon_2}^2}\right), \tag{12}$$

where,

$$Q_2(\boldsymbol{D}, \boldsymbol{\theta}) = \sum_{i=1}^{N-1} \sum_{j=i+1}^{N} (\text{TDoA}_m^{s_i-s_j} - \text{TDoA}_c^{s_i-s_j}(\boldsymbol{\theta}))^2$$

$N_t = (N-1)(N-2)/2$ is the total number of piezoelectrics triplet actuated by the same actuator. N is the total number of piezoelectric elements mounted into the structure.

5.2 Bayesian inference

For convenience, we will note in the sequel, $p(\boldsymbol{D}|\boldsymbol{\theta}, \sigma_{\epsilon}^2)$ without subscript 1 or 2 as in the likelihood function for both ToA and TDoA methods. Bayesian analysis relies on Bayes theorem, relating the joint prior parameter probability density function (PDF) $p_\pi(\boldsymbol{\theta}, \sigma_{\epsilon}^2)$ and the likelihood function $p(\boldsymbol{D}|\boldsymbol{\theta}, \sigma_{\epsilon}^2)$ to the joint posterior distribution $p(\boldsymbol{\theta}, \sigma_{\epsilon}^2|\boldsymbol{D})$ via

$$p(\boldsymbol{\theta}, \sigma_{\epsilon}^2|\boldsymbol{D}) = \frac{p(\boldsymbol{D}|\boldsymbol{\theta}, \sigma_{\epsilon}^2)p_\pi(\boldsymbol{\theta}, \sigma_{\epsilon}^2)}{p(\boldsymbol{D})} \tag{13}$$

Equation (13) provides us a simple means of relating prior information to the parameter distribution we seek. The term

$$p(\boldsymbol{D}) = \int p(\boldsymbol{D}|\boldsymbol{\theta}, \sigma_{\epsilon}^2)p_\pi(\boldsymbol{\theta}, \sigma_{\epsilon}^2)d\boldsymbol{\theta}d\sigma_{\epsilon}^2$$

in the demonimator, is a normalizing constant that can be ignored in the following development. The joint posterior parameter distribution contains the desired marginal distribution of each of the parameters vector. If we want to obtain the marginal distribution of a parameter θ_k (k = 1,2,3 or 4), part of $\boldsymbol{\theta}$, performing an integration of Equation (13) with respect to the variance σ_{ϵ}^2 and with respect to all the rest of parameters other than θ_k we have:

$$p(\theta_k|\boldsymbol{D}) \propto \int p(\boldsymbol{\theta}, \sigma_{\epsilon}^2|\boldsymbol{D})p_\pi(\boldsymbol{\theta}, \sigma_{\epsilon}^2)d\boldsymbol{\theta}_{-k}d\sigma_{\epsilon}^2 \tag{14}$$

where the notation $\int d\boldsymbol{\theta}_{-k}d\sigma_{\epsilon}^2$ denotes the multidimensional integral over all parameters other than θ_k. Solving Equation (14) would lead to an estimation of the update (posterior) distribution of the damage position and the angle dependent group velocity. Unfortunately, it is usually difficult to obtain an analytical solution of Equation (14) because of the very complicated expression of the likelihood function, and the high-dimensional integral involved. Fortunately there exists a convenient numerical approach to sampling from marginal parameter distributions. In this study, we used Markov Chain Monte Carlo (MCMC) methods for estimating the posterior distributions of the parameters.

5.3 Markov Chain Monte Carlo methods

Monte Carlo methods refer to simulation techniques for describing parameters in term of probability distribution, where samples are drawn from the marginal parameters distributions. These techniques can be highly efficient, especially when independent samples can be generated. Unfortunately, posterior distributions used in Bayesian inference are often complicated, making it difficult to draw independent samples. An alternative of using standard Monte Carlo methods is to use Markov Chain Monte Carlo (MCMC) simulation techniques. In this case, the new sample values are determined by using a few fixed number of previous samples values. The result of MCMC simulation is a dependent sequence of sample called a Markov chain. This Markov chain has stationary distributions equal to the distribution we wish to sample.

Metropolis-Hastings algorithm is a widely used technique for sampling from distributions for which the conditional densities cannot be computed, or are of a form from which it is difficult to sample (Bernardo and Smith, 1994). This technique uses a *proposal distribution*, from which sampling is easy, and accepts a sample with a probability that depends on the proposal distribution and the density from which we wish to sample. In this study, we applied joint Gibbs sampling (Bernardo and Smith, 1994) and Metropolis-Hastings algorithms as an alternative for sampling the full conditional distribution. The technique employed here is based on the rejection sampling and is detailed in the Appendix A.

6 Validation of the proposed parametric expression of the group velocity profile for the damage localization in a bayesian framework

As stated above, a model involving the wave group velocity that links the damage position and the ToFs is necessary to achieve accurate localization. An efficient and simple parametric modeling of the group velocity profile able to deal easily with anisotropy has been presented in the previous section. A Bayesian framework is considered to take into account for the facts that experimental times of flight are corrupted by noise and measurement errors and that variability of group velocity exists within composite materials. This section will now highlight in a bayesian framework the need to take into account for anisotropy in order to increase localization accuracy and thus the benefits associated with this simple model.

6.1 Numerical example

6.1.1 Illustrative case study

The specimen under study remains the same as in Section 4.1 with material properties listed in Table 1. The FEM of the composite plate is also the same as shown in Figure 3, with a damage located at (300,160) mm. The Bayesian approach is applied for both ToA and TDoA-based method and angle dependent (anisotropy) or independant (isotropy) velocity profiles using the ToF data collected from the scattered signal for each sensor. In the anisotropic case, the parameters vector is $\boldsymbol{\theta} = [x_d, y_d, a, b]$. Uniform prior are assumed for these parameters: x_d, y_d are uniformly distributed in [0,400] mm, [0,300] mm respectively, and wave velocity parameters a, b, are uniformly distributed in [0, 9000] m/s each. In the isotropic case, the parameters vector becomes $\boldsymbol{\theta} = [x_d, y_d, V_g]$, where uniform prior is assumed for $V_g \sim \mathcal{U}(0, 9000)$. It is worth mention that prior distributions on parameters a and b could be chosen using prior information gained by analyzing the damage pitch-catch free data (estimate of the velocity through least squares approach for example). This point will be illustrated later in the experimental study.

For each case and each parameter, a total of 120000 samples are considered to draw the Markov chain as shown in Figure 6(a) for damage location in the case of angle dependent group velocity.

The first 10000 are set as the burn-in period. The histogram of each estimated parameter exhibits a Gaussian trend as shown in Figure 6(b) and we thus used normal distribution to fit the histograms of each of the estimated MCMC parameters.
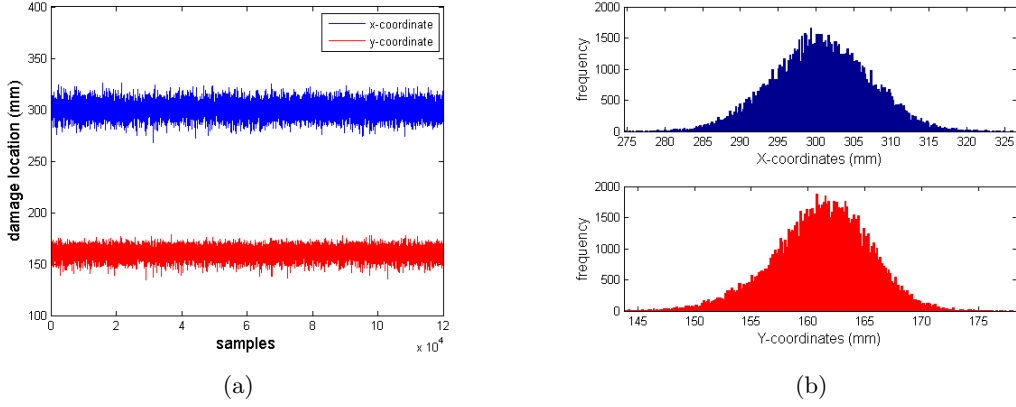

Figure 6: (a) MCMC samples for damage location (b) Histograms of MCMC samples for damage location-ToA: ellipse method - Anisotropy assumption in the group velocity (numerical study)

The estimated parameters as well as the confidence intervals and estimation errors are listed in Table 4 for the anisotropic case and in Table 5 for the isotropic case. The error for damage position is defined as the difference between the real damage position and the estimated damage position. For the group velocity parameters a and b, the relative error is defined as the difference between the estimated values and the actual values ($a = $ **5395.5 m/s** and $b = $ **4761.3 m/s** - see section 3.2) divided the actual values. For the velocity V_g in the isotropic case, no error can be defined as there exists no actual value. A zoomed 2D view of the damage location for the four cases is represented in Figure 7. The black circle represents the real damage location while PDF contour represents the estimated damage location.

Table 4: Estimation results and confidence intervals: numerical study (anisotropic case).

Parameter	ToA method				TDoA method			
	$x_d(mm)$	$y_d(mm)$	$a(m/s)$	$b(m/s)$	$x_d(mm)$	$y_d(mm)$	$a(m/s)$	$b(m/s)$
μ	300.6	161.1	5526	4420	293.1	156.3	5438	4779
σ	6.5	4.3	155.3	192.9	5.0	4.1	196	264
Error	-0.6	-1.10	-2.4 %	7.1 %	6.9	3.7	0.78 %	0.37 %

Table 5: Estimation results and confidence intervals: numerical study (isotropic case)

PDF param.	ToA method			TDoA method		
	$x_d(mm)$	$y_d(mm)$	$V_g(m/s)$	$x_d(mm)$	$y_d(mm)$	$V_g(m/s)$
μ	315.9	166.6	5426	311.6	167.6	6166
σ	7.1	6.4	159	4.6	3.9	190
Error (mm)	-15.9	-6.6	-	-11.6	-7.6	-

14

(a) Ellipse, anisotropy assumed.   (b) Hyperbol, anisotropy assumed.

(c) Ellipse, isotropy assumed.   (d) Hyperbol, isotropy assumed.
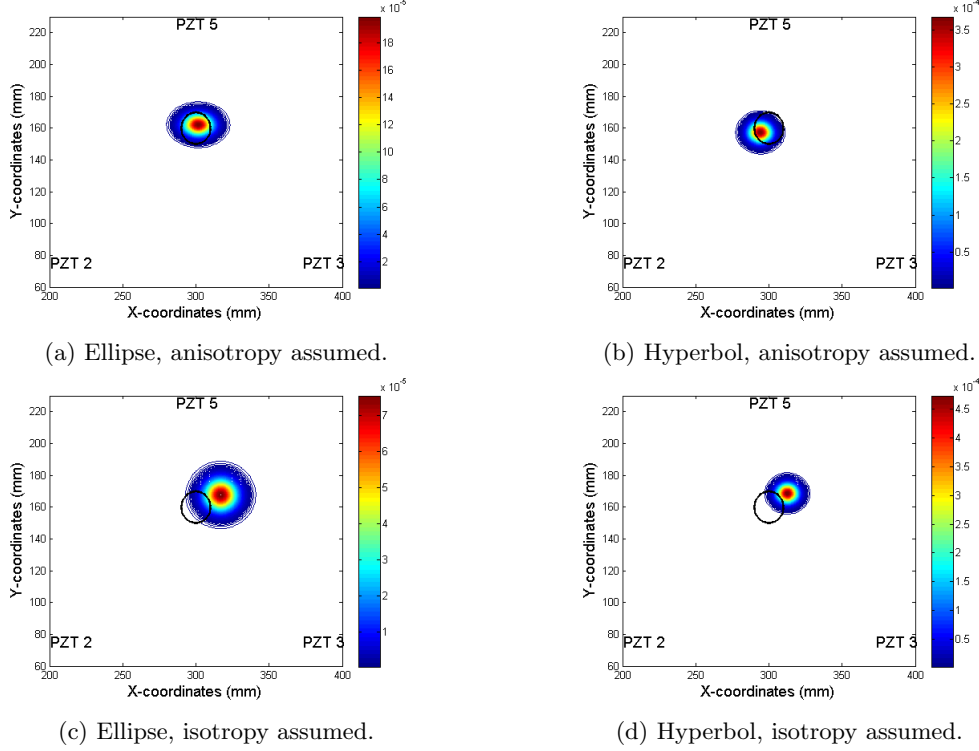
Figure 7: PDF of damage location for the four localization algorithms. Black circle represents true damage location.

One can observe from Table 4 that both localization methods (ToA, TDoA) give satisfying results for each estimated parameters. By comparing the results of Table 4 and Table 5, one can observe that taking into account the angle dependence of the wave velocity profile in the damage localization clearly increases localization accuracy. Figure 8 (a)(b) show the comparison between the actual and estimated group velocity profile for both case isotropy and anisotropy. For anisotropy assumption Figure 8 (a)(b), the group velocity profile is well estimated close to its actual profile with acceptable errors for both ToA and TDoA algorithms. This estimation become worst in the case of isotropy assumption (Figure 8 (c)(d)) as expected. This explains the failure of both algorithms relying on the isotropy assumption to provide an accurate damage localization for the present example.

6.1.2 Sensitivity to damage position

In order to further demonstrate the robustness of the proposed algorithm, we ran 5 other simulations with different damage locations, and computed statistics on the error. The objective of this approach is to show how sensitive the estimation is with respect to the changes in the damage location. The damage locations considered for this analysis are listed in Table 6. The estimation results with and without the anisotropy assumption are listed in Tables 7, 8 and 9,10 for both ellipse-based and hyperbola-based methods respectively. The root mean square error (RMSE) is

(a) Ellipse, anisotropy assumed.

(b) Hyperbol, anisotropy assumed.

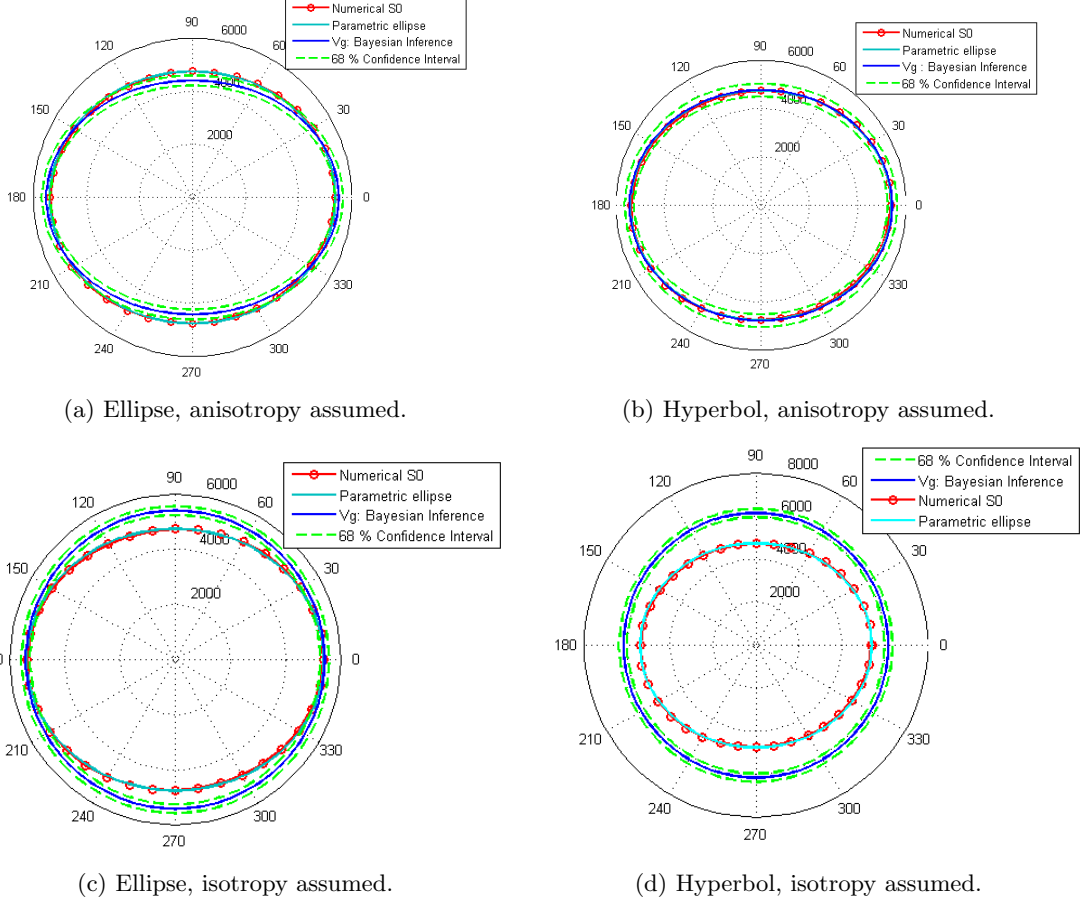(c) Ellipse, isotropy assumed.

(d) Hyperbol, isotropy assumed.

Figure 8: Group velocity profile and the associated Confidence Interval (CI): numerical study

also computed using the real damage location and the estimated damage location as follow:

$$\text{RMSE}(\hat{\theta}) = \sqrt{\mathbb{E}[(\hat{\theta} - \theta)^2]} \tag{15}$$

where, $\hat{\theta}$ is the estimated value and θ is the real value. The RMSE is a standard statistic metric used to measure estimator performance, and its value increases with the variance of the estimator.

Table 6: Damage coordinates for sensitivity analysis

Damages	D_1	D_2	D_3	D_4	D_5
x (mm)	100	150	150	200	250
y (mm)	150	150	200	150	100

From the results presented in Tables 7, 8, 9, 10 and in Figures 9 and 10 it can be observed that the proposed Bayesian approach leads to a good estimation in term of both damage location

16

Table 7: Estimated location and RMSE for each damage position: numerical study (Ellipse method, anisotropy assumption)

	D_1		D_2		D_3		D_4		D_5	
Coordinates	x_d	y_d	x_d	y_d	x_d	y_d	x_d	y_d	x_d	y_d
RMSE	12.2	8.6	8.8	10.1	9.5	7.6	16.6	8.1	6.8	9.8
Vg Param.	a	b	a	b	a	b	a	b	a	b
RMSE	195.3	493.7	152.2	183.7	260.9	304.7	369.4	481.4	235.5	320.4

Table 8: Estimated location and RMSE for each damage position: numerical study (Ellipse method, isotropy assumption)

	D_1		D_2		D_3		D_4		D_5	
Coordinates	x_d	y_d	x_d	y_d	x_d	y_d	x_d	y_d	x_d	y_d
RMSE	20.0	15.1	9.1	15.0	18.3	33.9	27.9	18.7	11.0	22.4
Vg Param.	a	b	a	b	a	b	a	b	a	b
RMSE	230.1	789.9	282.2	373.3	440.9	769.9	544.4	195.3	315.7	442.8

Table 9: Estimated location and RMSE for each damage position : numerical study (Hyperbola method, anisotropy assumption)

	D_1		D_2		D_3		D_4		D_5	
Coordinates	x_d	y_d	x_d	y_d	x_d	y_d	x_d	y_d	x_d	y_d
RMSE	44.4	10.1	3.7	7.5	12.4	8.5	7.1	8.0	6.0	13.4
Vg Param.	a	b	a	b	a	b	a	b	a	b
RMSE	1007.4	442.9	249.5	502.8	543.0	481.5	327.3	368.1	312.0	616.4

Table 10: Estimated location and RMSE for each damage position : numerical study (Hyperbola method, isotropy assumption)

	D_1		D_2		D_3		D_4		D_5	
Coordinates	x_d	y_d	x_d	y_d	x_d	y_d	x_d	y_d	x_d	y_d
RMSE	42.0	7.5	4.6	8.1	52.0	41.3	7.9	9.0	6.9	15.3
Vg Param.	a	b	a	b	a	b	a	b	a	b
RMSE	1077.6	443.4	189.4	548.1	833.1	1368.4	312.3	467.1	344.9	324.1

and group velocity profile. Indeed, the estimated parameters are in good agreement with the exact values for both ToA-based and TDoA-based methods, and for each damage location. For ToA-based algorithm and for the D4 damaged configuration, the RMSE for the parameter b in the isotropic model is higher than its value in the anisotropic assumption. This deviation is due to the high value of σ_b in the anisotropic model compared to its value in the isotropic case (see Tables 18-21 in appendix B), leading to high value of RMSE according to Equation 15. By choosing an estimator that has minimum variance, one also choose an estimator having minimum RMSE. It can been observed from the RMSE values listed in appendix B that the RMSE decreases with the variance for each of the estimated parameters. Although the hyperbola-based algorithm does not lead to a monotonic trend in terms of accuracy between isotropic and anisotropic assumption for each damaged case and for each estimated parameter, the proposed parametric group velocity model still performs well.
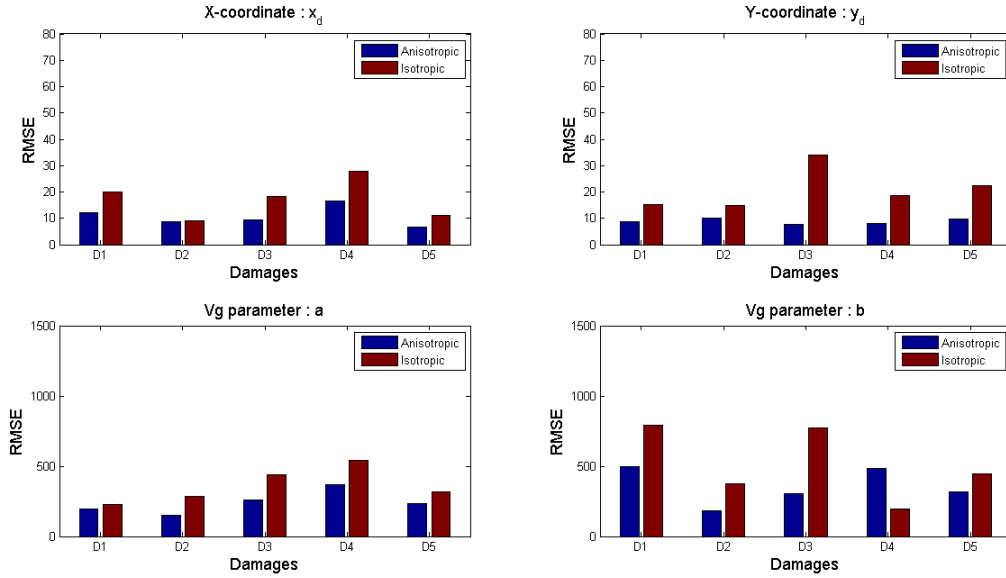
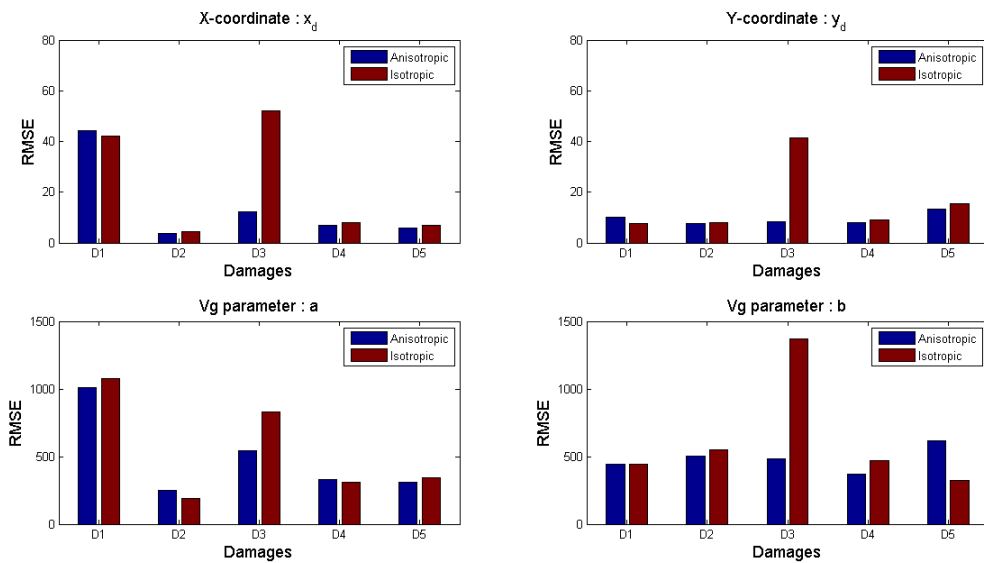Figure 9: RMSE of the estimated parameters, numerical study : ellipse method.

Figure 10: RMSE of the estimated parameters, numerical study : hyperbola method.

6.1.3 Sensitivity to changes in the anisotropy of the material

The sensitivity of the localization algorithm to a strong anisotropy is also analyzed in order to validate its applicability in a numerical framework. The material considered here exhibits a strong

anisotropy in one of the principal direction (along x axis). The material properties is listed in Table 11. The dimensions of the plate and the sensors location remain the same. The Lamb waves dispersion curve of this new material is shown in Figure 11. The parameters of the parametric ellipse model for the group velocity are estimated to be $\boldsymbol{a = 6092.9}$ **m/s** and $\boldsymbol{b = 4921.0}$ **m/s**.

Table 11: Mechanical properties of one ply of the new chosen composite material

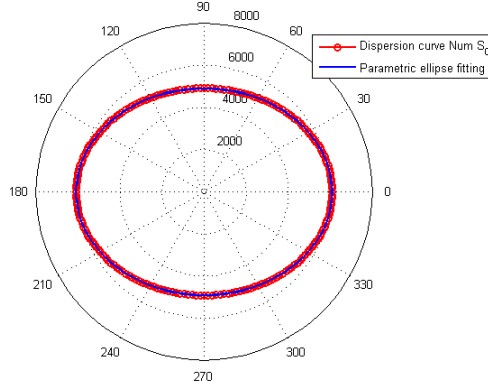| Density (g/m^3)	thickness (mm)	E_{11} (GPa)	E_{22} (GPa)	E_{33} (GPa)	$G_{12} = G_{13} = G_{23}$ (GPa)	ν_{12}
1554	0.28	80	40	8.1	4.8	0.03

Figure 11: Dispersion curve for the new material and its corresponding parametric fit

The previous described MCMC procedure was applied for damage localization in this new plate. The damage is located at (250,100) mm with 18 mm diameter. The estimated parameters are listed in Table 12 and 13 for both ToA-based and TDoA-based Bayesian Algorithm respectively, with and without taking into account for the anisotropy. The RMSE are plotted in Figure 12. The comparison between the RMSE and the estimated parameters values (μ and σ) in isotropic and anisotropic cases show that even for materials with strong anisotropy, the Bayesian damage localization performs well and the proposed parametric expression for the group velocity remains applicable and leads to results with acceptable errors.

Table 12: Estimation results and confidence intervals: numerical study (ToA-based algorithm).

Parameter	Anisotropic case				Isotropic case			
	$x_d(mm)$	$y_d(mm)$	$a(m/s)$	$b(m/s)$	$x_d(mm)$	$y_d(mm)$	$a(m/s)$	$b(m/s)$
μ	237.5	109.3	5978.1	4.936.9	233.9	103.2	5.7023	5.7023
σ	5.7	5.7	156.0	266.6	7.2	13.4	143.4	143.4
RMSE	13.6	10.9	193.7	267.0	17.6	13.8	416.1	794.3

19

Table 13: Estimation results and confidence intervals : numerical study (TDoA-based algorithm).

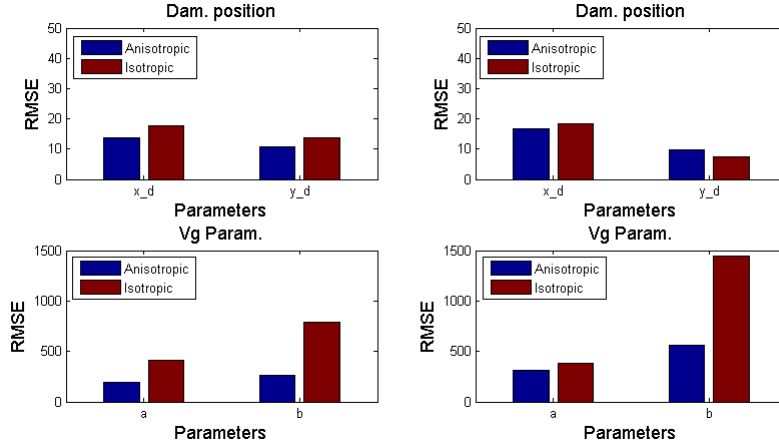| Parameter	Anisotropic case				Isotropic case			
	$x_d(mm)$	$y_d(mm)$	$a(m/s)$	$b(m/s)$	$x_d(mm)$	$y_d(mm)$	$a(m/s)$	$b(m/s)$
μ	233.8	108.1	6220.1	5227.9	231.9	96.4	6.3365	6.3365
σ	4.0	5.5	284.2	471.3	4.4	6.4	298.4	298.4
RMSE	16.7	9.8	311.3	562.4	18.5	7.3	385.2	1446.6

Figure 12: RMSE of the estimated parameters, numerical study : (left) ellipse method, (right) hyperbola method

6.2 Experimental application : composite laminate

6.2.1 Experimental setup

To further illustrate the effectiveness of the proposed algorithm, experimental studies are conducted on a composite plate. The test specimen is a 4 plies composite plate with plies orientation $[0°/ - 45°/45°/0°]$. The dimensions of the laminate is 400 mm $\times$ 300 mm $\times$ 1.2 mm as in the numerical study. Mechanical properties of the lamina are listed in Table 14. A set of $N = 5$ piezoelectric elements (Noliac NCE51) from NOLIAC Inc., each with a diameter of 20 mm and thickness of 0.1 mm are surface mounted on the composite plate. The sensor placement is the same as in the numerical study (see Section 4.1).

Table 14: Mechanical properties of the lamina in the experimental study

Density (g/m^3)	ply thickness (mm)	$E_{11} = E_{22}$ (GPa)	E_{33} (GPa)	$G_{12} = G_{13} = G_{23}$ (GPa)	ν_{12}
1554	0.28	69	8.1	4.8	0.03

The experimental setup is shown in Figure 13(a). The excitation signal is a 5 cycles sinusoidal tone burst with a central frequency of $f_0 = 200$ kHz, modulated by a Hanning window, as previously. The excitation signal is generated by a 33500B series Waveform Generator, and amplified to 10 V using a voltage amplifier from FLC Electronics. The sensors signals are visualized and

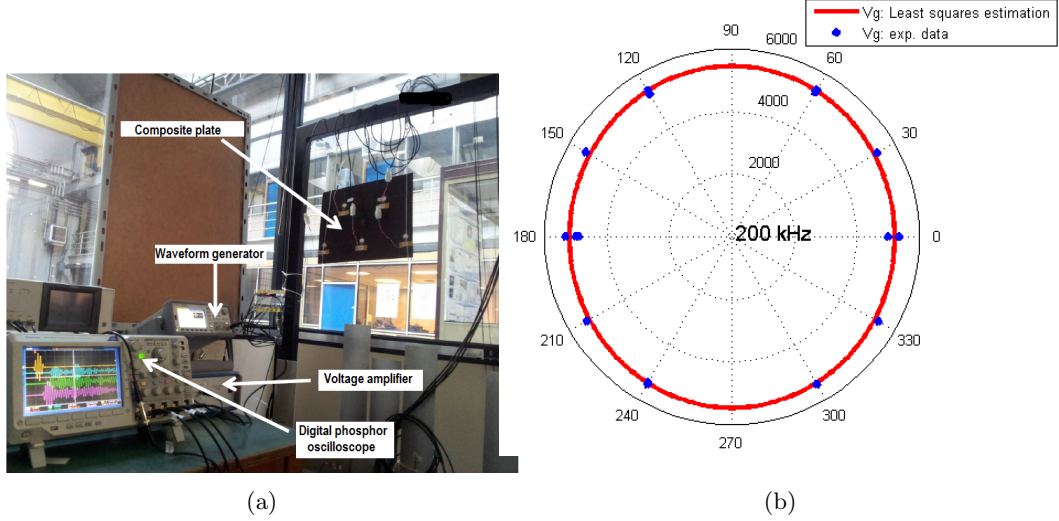recorded by a Tektronix Digital Phosphor Oscilloscope (DPO3014 series) whose sampling rate is set at 25 MHz.

Figure 13: Experimental setup (a), parametric ellipse construction with experimental group velocity in composite $[0°/-45°/45°/0°]$ ply laminate at 200 kHz: least-squares fitting (b)

After the recording of the signals for the healthy plate, the group velocity can be estimated for several propagation angles using the ToF method. Figure 13(b) shows the experimental group velocity data points as well as the parametric ellipse fitted to these points. The values of the parameters **a** and **b** are estimated by a least-squares method, and are: **5214.4 m/s** and **5472.6 m/s** respectively. One can observe in Figure 13(b) a good match between experimental data and least-squares estimation results using these values. One can also observe that material used here is not as anisotropic as the one used in the numerical simulations.

The two damages considered in this study are impacts with diameters of 14 mm and 22 mm. These impacts are calibrated damages, obtained using a Drop Weight Impact Test System. Figures 14(a) and 15(a) show the composite plate with the impacts. Damage characterization was performed using ultrasonic non destructive testing (NDT) before and after the impact as shown in the figures. The damage is at the opposite face to which the transducer elements are bounded. The center location of the 14 mm damaged impact is at (300,150) mm and the center location of the 22 mm damaged impact is at (100,150). Figure 14(b) and Figure 15(b) illustrates the damaged composite plate with sensors placement and the damages location. After recording the signals from the healthy and damaged plates, a signal scattered by damage is obtained and the procedure described in Section 2.1 is used to obtain the ToFs for each damage case.

6.2.2 Results for the 14 mm impact damage

In the anisotropic case, the posterior distributions of the parameters vector $\boldsymbol{\theta} = [x_d, y_d, a, b]$ is estimated by the previously described MCMC procedure. Uniform prior are assumed for each parameter. That is x_d, y_d are uniformly distributed in [0,400] mm, [0,300] mm respectively, and wave velocity parameters a, b, are uniformly distributed in [0, 8000] m/s each. For each case and each parameter, a total of 120000 samples are considered to draw the Markov chain. The
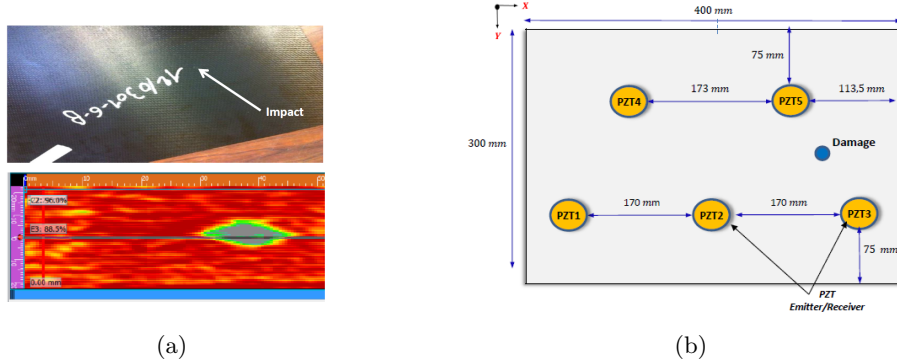
Figure 14: (a) Composite plate with the 14 mm impact (top) C-scan of the impact (bottom), (b) Coordinates of the impact (300,150)mm.
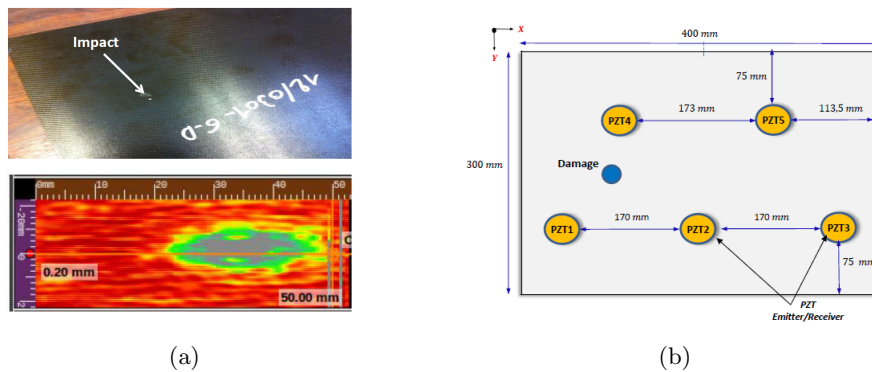

Figure 15: (a) Composite plate with the 22 mm impact (top) C-scan of the impact (bottom), (b) Coordinates of the impact (100,150)mm.

first 10000 are set as the burn-in period. The histogram of each estimated parameter exhibits a Gaussian trend as shown in Figure 16(b) and we thus used normal distribution to fit the histograms of each of the estimated MCMC parameters. The estimated parameters as well as the estimation errors and confidence intervals are listed in Table 15. The error are defined as previously. 2D view of the damage location estimates for the different cases that are considered are represented in Figure 17. The black circle represents the real damage (impact) location while PDF contour represents the estimated damage location.

One can observe from Table 15 that both localization methods (ToA, TDoA) give satisfying results with acceptable errors for each estimated parameters. These results further demonstrate the effectiveness of the proposed Bayesian damage localization based on the parametric expression of the wavefront.

6.2.3 Result for the 22 mm impact damage

The same procedure as in the previous damaged case is followed here. The estimated parameters as well as the estimation errors and confidence intervals are listed in Table 16. 2D view of the damage location is represented in Figure 18. The black circle represents the real damage (impact)
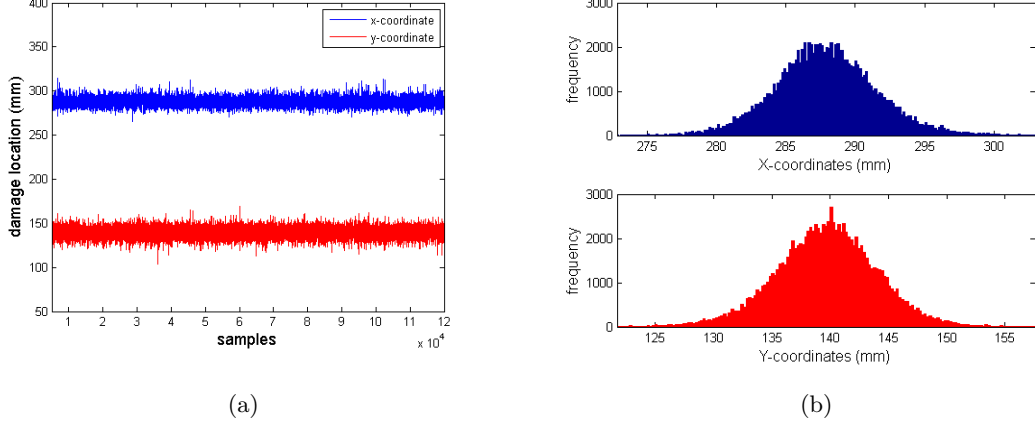
22

Figure 16: Experimental Results for composite plate: (a) MCMC samples for damage location (14 mm) (b) Histograms of MCMC samples for damage location - ToA: ellipse method - Anisotropy assumption in the group velocity

Table 15: Estimation results and confidence intervals for composite plate - 14 mm.

PDF param.	ToA method				TDoA method			
	$x_d(mm)$	$y_d(mm)$	$a(m/s)$	$b(m/s)$	$x_d(mm)$	$y_d(mm)$	$a(m/s)$	$b(m/s)$
μ	287.8	139.6	5085	5440	290.6	140.1	5269	5092
σ	3.7	4.5	107	170	8.9	5.0	499	306
Error	12.2	10.4	2.4 %	0.6 %	9.4	9.9	-1.05 %	6.9 %

location while PDF contour represents the estimated damage location. Table 16 further shows that the proposed damage localization method give satisfying results with acceptable error for both algorithms.

Table 16: Estimation results and confidence intervals for composite plate - 22 mm.

PDF param.	ToA method				TDoA method			
	$x_d(mm)$	$y_d(mm)$	$a(m/s)$	$b(m/s)$	$x_d(mm)$	$y_d(mm)$	$a(m/s)$	$b(m/s)$
μ	115.1	160.2	5325	5803	114.2	160.9	5038	5300
σ	3.9	3.2	81	118	3.6	2.5	255	157
Error	-15.1	-10.2	-2.1 %	-6.0 %	-14.2	-10.9	3.4 %	3.1 %

6.3 Experimental application : sandwich structure

6.3.1 Experimental setup

Another experimental study is conducted on a sandwich structure to validate the proposed algorithm. The test specimen is a sandwich plate. The face sheets are made of the previous described 4 plies composite plate with plies orientation $[0°/-45°/45°/0°]$, and the core is made of aluminum. The dimensions of the sandwich plate is 400 mm × 300 mm × 30.2 mm. 5 piezoelectric elements from Noliac NCE51 were bonded to the sandwich plate according to the same configuration as

(a) Ellipse

(b) Hyperbola

Figure 17: Experimental Results for composite plate: PDF of damage location- 2D view (a) ToA: ellipse method (b) TDoA: hyperbola method. Black circle represents true damage location
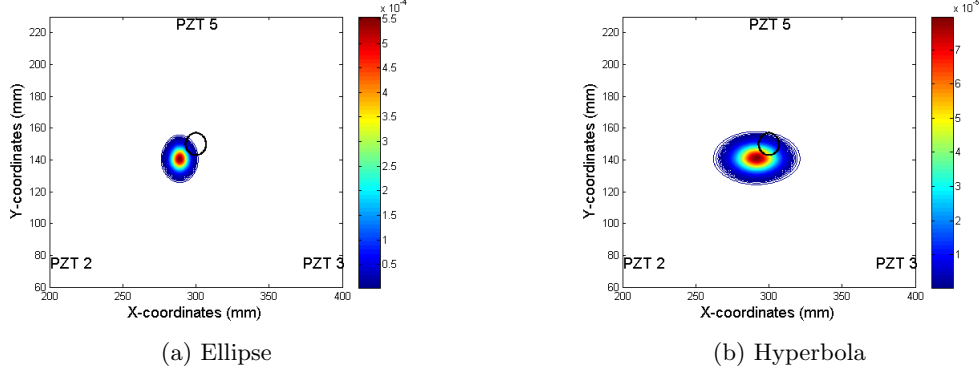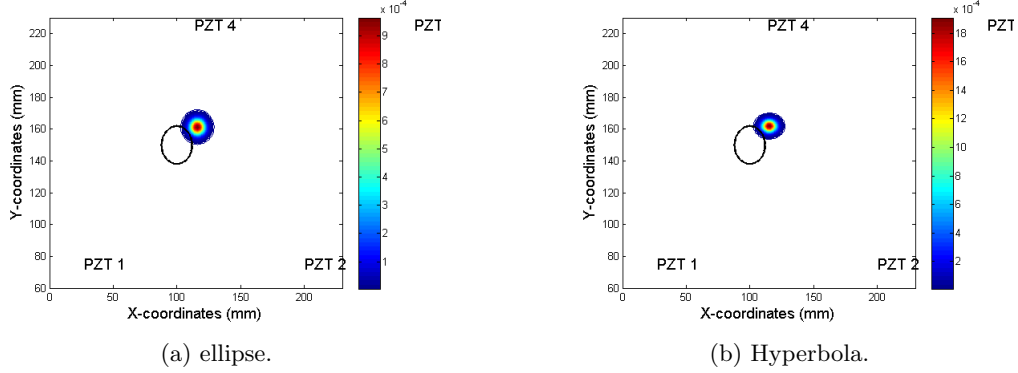

(a) ellipse.

(b) Hyperbola.

Figure 18: Experimental Results for composite plate: PDF of damage location- 2D view (a) ToA: ellipse method (b) TDoA: hyperbola method. Black circle represents true damage location

in the previous experimental case. The sensors placement, the mechanical properties of the face sheets for the sandwich plate and the dimensions of the plate are the same as in the previous study case.

The excitation signal in this case is a 5 cycles sinusoidal tone burst with a central frequency of $f_0 = 50$ kHz, modulated by a Hanning window, as previously. The amplitude is set to 10 V, and the sampling rate at 10 MHz.

After recording the signals for the healthy sandwich plate, the group velocity can be estimated for several propagation angles using the ToF method. As in the previous experimental study, the experimental group velocity data points as well as the parametric ellipse fitted to these points were plotted in Figure 19(b) for the sandwich structure. The values of the parameters a and b are estimated by a least-squares method, and are: **4282.5 m/s** and **4411.4 m/s** respectively. As shown in the figure, the group velocity profile exhibits a quasi-circular shape with a relatively high variance. The MCMC procedure will be used to quantify the uncertainties associated to this estimation.

For Bayesian damage localization we consider an impact with diameters of 18 mm. As in the
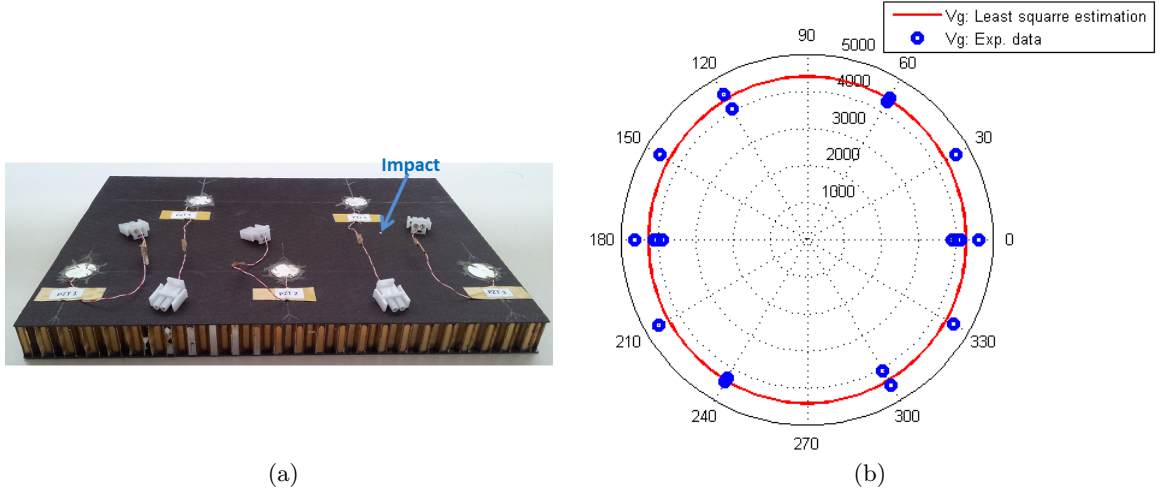
24

<center>(a)</center> <center>(b)</center>

Figure 19: Sandwich plate with a impact (a), parametric ellipse construction with experimental group velocity in sandwich plate at 50 kHz: least-squares fitting (b)

previous case, The impact is a calibrated damage, obtained using a Drop Weight Impact Test System. Figure 19(a) shows the sandwich plate with the impact. The damage is at the opposite face to which the transducer elements are bounded. The center location of the 18 mm damaged impact is at (303,150) mm. After recording the signals from the healthy and damaged plates, a signal scattered by damage is obtained and the procedure described in Section 2.1 is used to obtain the ToFs.

6.3.2 Results for the 18 mm impact damage on sandwich plate

The MCMC procedure was applied to this new damaged case. We used normal distribution prior for the group velocity parameters a and b, with mean values, those obtained by the least squares methods (see Section 6.3.1), and the associated variance is equal to the variance of the experimental data. The MCMC histograms and 2D view of the damage location are represented in Figures 20 and 21 respectively. The black circle represents the real damage (impact) location while PDF contour represents the estimated damage location. Table 17 further shows that the proposed damage localization method give satisfying results with acceptable error for both algorithms.

<center>Table 17: Estimation results and confidence intervals for sandwich plate - 18 mm.</center>

	ToA method				TDoA method			
PDF param.	$x_d(mm)$	$y_d(mm)$	$a(m/s)$	$b(m/s)$	$x_d(mm)$	$y_d(mm)$	$a(m/s)$	$b(m/s)$
μ	283.0	130.9	4534.4	4160.2	316.3	174.9	4132	4639
σ	11.8	20.9	224.6	330.3	16.07	28.8	525.7	475.4
Error	20	19.1	-5.89 %	5.68 %	13.3	24.9	3.5 %	-5.16%

7 Conclusions

This paper focuses on probabilistic Lamb wave-based damage localization in anisotropic composite materials and the three following points were addressed in this context:
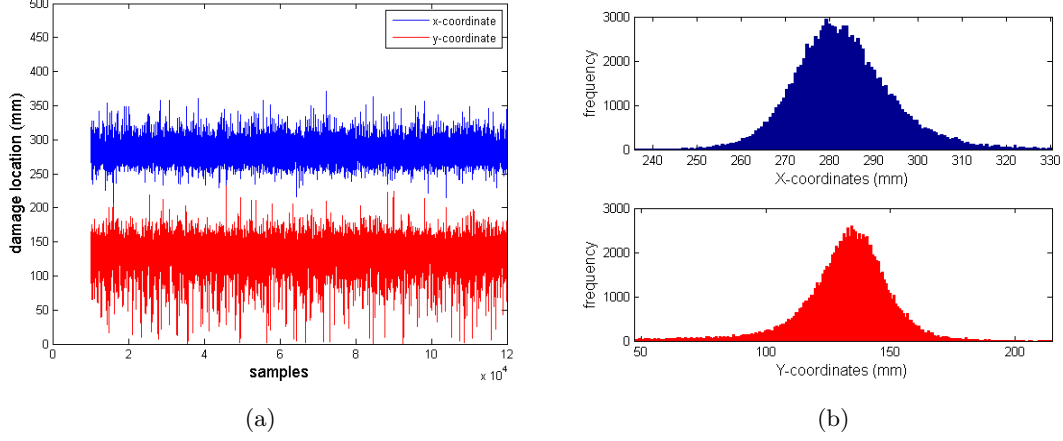
<center>25</center>

Figure 20: Experimental Results for sandwich plate : (a) MCMC samples for damage location (18 mm) (b) Histograms of MCMC samples for damage location - ToA: ellipse method - Anisotropy assumption in the group velocity

Figure 21: Experimental Results for sandwich plate: PDF of damage location- 2D view (a) ToA: ellipse method (b) TDoA: hyperbola method. Black circle represents true damage location

- The use of a Bayesian framework in order to take into account for both measurement and material uncertainties in an anisotropic context

- The development and validation of an efficient and simple parametric modeling of the group velocity profile in order to deal easily with anisotropy.

- The influence of the use of ToA of DToA on localization accuracy.

- The influence of both the damage location and the strong anisotropy of the material in the estimation results.

A Bayesian framework is considered to take into account for the facts that experimental ToFs are corrupted by noise and the variability of group velocity exists within composite materials. An

original parametric analytical expression of the direction dependence group velocity is proposed and validated numerically and experimentally for anisotropic composite plates and sandwich structure. This expression is incorporated into time-of-arrival (ToA: ellipse-based) and time-difference-of-arrival (TDoA: hyperbola-based) bayesian damage localization algorithms. This way, the damage location as well as the group velocity profile are estimated jointly. On the basis of the framework developed by Yan (2013), we have proposed and validated numerically and experimentally a general localization algorithm that allows (i) to take into account for for both measurement and material uncertainties within a Bayesian framework, (ii) to model easily the effects of anisotropy on group velocity and, (iii) to rely on ToA or TDoA informations. The original feature of this approach is that it incorporates anisotropic wave propagation via a parametrized analytic expression of the angle dependence of the wave velocity profile in the Bayesian localization model and allows to use both ToA and TDoA algorithms. Numerical and experimental results obtained with different damage sizes and locations validate the ability of the proposed algorithm to estimate both the damage location and the group velocity profile as well as the associated confidence intervals. Results highlight the need to take into account for anisotropy in order to increase localization accuracy. In addition to the anisotropic model used for localization, the Bayesian approach is more effective than the classical imaging algorithms in term of uncertainties quantification as shown by the obtained results. The overall performance shows that ToA-based algorithm leads to better results in comparison to TDoA-based algorithm.

Acknowledgments

Appendix

A   Metropolis-Hastings Algorithm

Suppose that we wish to draw samples from a specific distribution $f(\theta)$ (in our case, $f(\theta)$ is $p(\theta_k|\boldsymbol{D})$ in Equation (14)). The Metropolis-Hastings algorithm generates a sequence $\{\theta^{(i)}\}$ by a 2-step procedure. At stage i a candidate value θ^* is sampled based on the current value $\theta^{(i-1)}$; it is sampled from a distribution function $g(x|\theta^{(i-1)})$. Then a Bernoulli trial is performed with success probability:

$$r' = \min\{\frac{f(\theta^*)g(\theta^{(i-1)}|\theta^*)}{f(\theta^{(i-1)})g(\theta^*|\theta^{(i-1)})},1\} \tag{16}$$

if the result of the trial is success, we set $\theta^{(i)} = \theta^*$; otherwise we set $\theta^{(i)} = \theta^{(i-1)}$. More often practice considers a candidate generating distribution which is symmetric in its arguments, that is $g(\theta^{(i-1)}|\theta^*) = g(\theta^*|\theta^{(i-1)})$. If we consider uniform distribution proposal for a candidate θ^* on an interval of length $2A$ centered on $\theta^{(i-1)}$, then density function is:

$$g(\theta^*|\theta^{(i-1)}) = \frac{1}{2A}, \qquad |\theta^* - \theta^{(i-1)}| < A. \tag{17}$$

In a such case, the acceptance probability r' reduces to:

$$r' = \min\{\frac{f(\theta^*)}{f(\theta^{(i-1)})},1\} \tag{18}$$

Practical implementation of the MCMC algorithm can require some tuning of the interval length A in Equation (17). Large values of A reduces the acceptance ratio, and the Markov chain tends

to be highly correlated. Low values of A leads to important convergence time. A trade-off between these two aspects is well known. We used in this study an approach proposed by (Nichols et al., 2010), where the value of A is adjusted in the "burn-in" period.

Uniform transition distribution (proposal distribution) were used in this study. The MCMC algorithm for generating posterior parameters distribution in Equation (14) is described in Appendix.

- set the number of total iterations N_{iter} and the number of "burn-in" N_B

- choose initial guesses $\theta_k^{(0)}$, $k = 1, ..., p$

- choose initial tuning parameter A_k, $k = 1, ..., p$

- sample initial variance noise from an inverse gamma (IG) distribution: $\sigma_\epsilon^2(0) = IG(N_m/2 + 1, Q(\boldsymbol{D}, \boldsymbol{\theta}^{(0)})/2)$

Main iteration : increment i by 1 and do:

For each parameter k, $\quad k = 1 : p$

- Generate a candidate $\theta_k^* = \theta_k^{(i-1)} + 2A_k \times \mathcal{U}(-1, 1)$, where $\mathcal{U}(-1, 1)$ is a uniformly distributed number on [-1,1].

- compute:

$$r' = \exp\left[-(0.5/\sigma_\epsilon^2(i-1)) \times (Q(\boldsymbol{D}, \boldsymbol{\theta}^*) - Q(\boldsymbol{D}, \boldsymbol{\theta}^{(i-1)}))\right] \times p_{\pi_k}(\boldsymbol{\theta}^*)/p_{\pi_k}(\boldsymbol{\theta}^{(i-1)})$$

  where: $\quad \boldsymbol{\theta}^* = [\theta_1^{(i)}, ..., \theta_{(k-1)}^{(i)}, \theta_k^*, \theta_{(k+1)}^{(i-1)}, ..., \theta_p^{(i-1)}]$
  and: $\quad \boldsymbol{\theta^{(i-1)}} = [\theta_1^{(i)}, ..., \theta_{(k-1)}^{(i)}, \theta_k^{(i-1)}, \theta_{(k+1)}^{(i-1)}, ..., \theta_p^{(i-1)}]$

    - if $\mathcal{U}(0, 1) < r'$, keep the new value $\theta_k^{(i)} = \theta_k^*$ and adjust tuning parameter $A_k = A_k \times 1.01$
    - else reject the new value and keep $\theta_k^{(i)} = \theta_k^{(i-1)}$ and adjust the tuning parameter $A_k = A_k/1.007$

- direct sample the variance posterior distribution $\sigma_\epsilon^2(i) = IG(N_m/2 + 1, Q(\boldsymbol{D}, \boldsymbol{\theta}^{(i)})/2)$, and do $i = i + 1$

- after $i > N_B$ cease adjusting the tuning parameter A_k.

- repeat procedure until $i = N_{iter}$

After discarding the N_B values corresponding to the burn-in period, the resulting Markov chain of parameter θ_k has a stationary distribution that tends to the target distribution $p(\theta_k|\boldsymbol{D})$.

B Root mean square error: numerical results

Table 18: Numerical results: estimated location and RMSE for each damage position (Ellipse method, anisotropic assumption)

	D₁		D₂		D₃		D₄		D₅	
Coordinates	x_d	y_d	x_d	y_d	x_d	y_d	x_d	y_d	x_d	y_d
Estimation (mm)	90.6	144.9	142.6	140.5	144.3	201.9	214.6	152.1	248.8	104.0
σ (mm)	7.8	6.9	4.8	3.5	7.6	7.4	7.8	7.8	6.7	8.9
Exact Pos. (mm)	100	150	150	150	150	200	200	150	250	100
RMSE	12.2	8.6	8.8	10.1	9.5	7.6	16.6	8.1	6.8	9.8
Vg Param.	a	b	a	b	a	b	a	b	a	b
Estimation (m/s)	5442.0	5134.9	5392.6	4678.2	5394.6	4595.8	5104.5	4398.7	5296.2	4694.1
σ (m/s)	189.7	322.8	152.2	163.9	260.9	255.9	227.5	316.7	213.5	313.3
Exact Value(m/s)	5395.5	4761.3	5395.5	4761.3	5395.5	4761.3	5395.5	4761.3	5395.5	4761.3
RMSE	195.3	493.7	152.2	183.7	260.9	304.7	369.4	481.4	235.5	320.4

Table 19: Numerical results: estimated location and RMSE for each damage position (Ellipse method, isotropic assumption)

	D₁		D₂		D₃		D₄		D₅	
Coordinates	x_d	y_d	x_d	y_d	x_d	y_d	x_d	y_d	x_d	y_d
Estimation (mm)	82.1	138.5	142.7	135.8	139.8	225.9	226.3	158.0	246.7	98.9
σ (mm)	8.8	9.9	5.4	4.9	15.1	21.8	9.2	16.9	10.5	22.4
Exact Pos. (mm)	100	150	150	150	150	200	200	150	250	100
RMSE	20.0	15.1	9.1	15.0	18.3	33.9	27.9	18.7	11.0	22.4
Vg Param.	a	b	a	b	a	b	a	b	a	b
Estimation (m/s)	5528.6	5528.6	5125.5	5125.5	5392.5	5392.5	4874.8	4874.8	5154.4	5154.4
σ (m/s)	187.7	187.7	82.0	82.0	440.9	440.9	158.9	158.9	203.9	203.9
Exact Value(m/s)	5395.5	4761.3	5395.5	4761.3	5395.5	4761.3	5395.5	4761.3	5395.5	4761.3
RMSE	230.1	789.9	282.2	373.3	440.9	769.9	544.4	195.3	315.7	442.8

Table 20: Numerical results: estimated location and RMSE for each damage position (Hyperbola method, anisotropic assumption)

	D₁		D₂		D₃		D₄		D₅	
Coordinates	x_d	y_d	x_d	y_d	x_d	y_d	x_d	y_d	x_d	y_d
Estimation (mm)	144.4	159.9	151.4	142.6	140.9	195.7	206.6	142.4	253.7	111.4
σ (mm)	1.3	1.7	3.4	1.7	8.5	7.3	2.7	2.6	4.7	7.0
Exact Pos. (mm)	100	150	150	150	150	200	200	150	250	100
RMSE	44.4	10.1	3.7	7.5	12.4	8.5	7.1	8.0	6.0	13.4
Vg Param.	a	b	a	b	a	b	a	b	a	b
Estimation (m/s)	4389.1	4934.8	5204.0	4840.1	5760.4	4863.9	5405.6	5095.9	5451.3	5120.9
σ (m/s)	44.9	407.6	160.0	496.6	402.1	470.4	327.11	213.9	306.9	500.6
Exact Value(m/s)	5395.5	4761.3	5395.5	4761.3	5395.5	4761.3	5395.5	4761.3	5395.5	4761.3
RMSE	1007.4	442.9	249.5	502.8	543.0	481.5	327.3	368.1	312.0	616.4

Table 21: Numerical results: estimated location and RMSE for each damage position (Hyperbola method, isotropic assumption)

	D$_1$		D$_2$		D$_3$		D$_4$		D$_5$	
Coordinates	x_d	y_d	x_d	y_d	x_d	y_d	x_d	y_d	x_d	y_d
Estimation (mm)	142.0	157.5	152.6	142.1	110.2	225.7	207.2	141.5	254.1	112.9
σ (mm)	0.3	0.1	3.7	2.1	33.5	32.2	3.2	3.0	5.5	8.2
Exact Pos. (mm)	100	150	150	150	150	200	200	150	250	100
RMSE	42.0	7.5	4.6	8.1	52.0	41.3	7.9	9.0	6.9	15.3
Vg Param.	a	b	a	b	a	b	a	b	a	b
Estimation (m/s)	4318.0	4318.0	5287.0	5287.0	6007.5	6007.5	5173.5	5173.5	5513.5	5513.5
σ (m/s)	13.2	13.2	155.2	155.2	565.2	565.2	219.7	219.7	324.1	304.15
Exact Value(m/s)	5395.5	4761.3	5395.5	4761.3	5395.5	4761.3	5395.5	4761.3	5395.5	4761.3
RMSE	1077.6	443.4	189.4	548.1	833.1	1368.4	312.3	467.1	344.9	324.1

References

Balmes E (2014) *Structural Dynamics Toolbox (for use with MATLAB)* . www.sdtools.com.

Balmes E, Guskov M, Rébillat M, et al. (2014) Effects of temperature on the impedance of piezoelectric actuators used for SHM. In :*Vibrations Shocks and Noise* 17-19 juin 2014, Vishno Aix-en-Provence, France pp. 1–6.

Beck J and Au S (2002) Bayesian updating of structural models and reliability using markov chain monte carlo simulation. *Journal of Engineering Mechanics* **128**(4), 380–391.

Beck J and Katafygiotis L (1998) Updating models and their uncertainties. part i: Bayesian statistical framework. *Journal of Engineering Mechanics* **124**(4), 455–461.

Bernardo J and Smith A (1994) *Bayesian Theory.* Wiley,Chichester.

Ciampa F and Meo M (2010) A new algorithm for acoustic emission localization and flexural group velocity determination in anisotropic structures. *Composites Part A: Applied Science and Manufacturing* **41**(12), 1777 – 1786.

Coverley P and Staszewski W (2003) Impact damage location in composite structures using optimized sensor triangulation procedure. *Smart Materials and Structures* **12**(5), 795.

Farrar C, Duffey T, Deobling S, et al. (1999) A statistical pattern recognition paradigm for vibration-based structural health monitoring. In :*2nd International Workshop on Structural Health Monitoring* Stanford, CA, 8-10 September 2000 pp 76473.

Flynn E and Todd M (2010) A bayesian approach to optimal sensor placement for structural health monitoring with application to active sensing. *Mechanical Systems and Signal Processing* **24**(4), 891 – 903.

Flynn E, Todd M, Wilcox P, et al. (2011) Maximum-likelihood estimation of damage location in guided-wave structural health monitoring. In :*Proceedings of The Royal Society A* Vol. 467 p. 257596.

Giurgiutiu V (2005) Tuned lamb wave excitation and detection with piezoelectric wafer active sensors for structural health monitoring. *Journal of Intelligent Material Systems and Structures* **16**(4), 291–305.

Hajzargerbashi T, Kundu T and Bland S (2011) An improved algorithm for detecting point of impact in anisotropic inhomogeneous plates. *Ultrasonics* **51**(3), 317 – 324.

Ihn J and Chang F (2008) Pitch-catch active sensing methods in structural health monitoring for aircraft structures. *Structural Health Monitoring* **7**(1), 5–19.

Jeong H and Jang Y.-S (2000) Wavelet analysis of plate wave propagation in composite laminates. *Composite Structures* **49**(4), 443 – 450.

Jiang X and Mahadevan S (2008) Bayesian wavelet methodology for structural damage detection. *Structural Control and Health Monitoring* **15**(7), 974–991.

Karandikar J, Kim N and Schmitz T (2012) Prediction of remaining useful life for fatigue-damaged structures using bayesian inference. *Engineering Fracture Mechanics* **96**(0), 588–605.

Kundu T, Das S and Jata K (2007) Point of impact prediction in isotropic and anisotropic plates from the acoustic emission data. *Acoustical Society of America* **122**, 2057.

Kundu T, Nakatani H and Takeda N (2012) Acoustic source localization in anisotropic plates. *Ultrasonics* **52**(6), 740 – 746.

Li B, Liu Y, Gong K, et al. (2013) Damage localization in composite laminates based on a quantitative expression of anisotropic wavefront. *Smart Materials and Structures* **22**(6), 065005.

Lin X and Yuan F (2001) Damage detection of a plate using migration technique. *Journal of Intelligent Material Systems and Structures* **12**(7), 469–482.

Lu Y, Ye L and Su Z (2006) Crack identification in aluminium plates using lamb wave signals of a pzt sensor network. *Smart Materials and Structures* **15**(3), 839.

Macea B, Duhamel D, Brennan J, et al. (2005) Finite element prediction of wave motion in structural waveguides. *Acoustical Society of America* **117**(5), 28352843.

Michaels J (2008) Detection, localization and characterization of damage in plates with an in situ array of spatially distributed ultrasonic sensors. *Smart Materials and Structures* **17**(3), 035035.

Moll J, Schulte R, Hartmann B, et al. (2010) Multi-site damage localization in anisotropic plate-like structures using an active guided wave structural health monitoring system. *Smart Materials and Structures* **19**(4), 045022.

Nichols J, Link W, Murphy K, et al. (2010) A bayesian approach to identifying structural non-linearity using free-decay response: Application to damage detection in composites. *Journal of Sound and Vibration* **329**(15), 2995 – 3007.

Niethammer M, Jacobs L, Qu J, et al. (2001) Time-frequency representations of lamb waves . *Acoustical Society of America* **109**(4), 1841.

Niri E, Farhidzadeh A and Salamone S (2013) Adaptive multisensor data fusion for acoustic emission source localization in noisy environment. *Structural Health Monitoring* **12**(1), 59–77.

Niri E and Salamone S (2012) A probabilistic framework for acoustic emission source localization in plate-like structures. *Smart Materials and Structures* **21**(3), 035009.

Raghavan A and Cesnik C (2007) Guided-wave signal processing using chirplet matching pursuits and mode correlation for structural health monitoring. *Smart Materials and Structures* **16**(2), 355.

Sohn H, Farrar C, Hemez F, et al. (2003) *A Review of Structural Health Monitoring Literature:1996-2001.* Los Alamos National Laboratory Report.

Sorohan S, Constantin N, Gvan M, et al. (2011) Extraction of dispersion curves for waves propagating in free complex waveguides by standard finite element codes. *Ultrasonics* **51(4):503-15**(4).

Su Z and Ye L (2009) *Identification of Damage Using Lamb Waves.* Springer.

Tua P, Quek S and Wang Q (2004) Detection of cracks in plates using piezo-actuated lamb waves. *Smart Materials and Structures* **13**(4), 643.

Vanik M, Beck J and Au S (2000) Bayesian probabilistic approach to structural health monitoring. *Journal of Engineering Mechanics* **126**(7), 738–745.

Xu B, Yu L and Giurgiutiu V (2009) Advanced methods for time-of-flight estimation with application to lamb wave structural health monitoring. In : *7th International Workshop on Structural Health Monitoring* Stanford University, Palo Alto, CA pp. 1202–1209.

Yan G (2013) A bayesian approach for damage localization in plate-like structures using lamb waves. *Smart Materials and Structures* **22**(3), 035012.

Yu L, Leckey L and Cara A (2012) Lamb wavebased quantitative crack detection using a focusing array algorithm. *Journal of Intelligent Material Systems and Structures* .

Yu L and Su Z (2012) Application of kernel density estimation in lamb wave-based damage detection. *Mathematical Problems in Engineering* **2012**, no.406521.

Zhao X, Gao H, Zhang G, et al. (2007) Active health monitoring of an aircraft wing with embedded piezoelectric sensor/actuator network: I. defect detection, localization and growth monitoring. *Smart Materials and Structures* **16**(4), 1208.